Received: 6 December 2023 | Revised: 12 February 2024 | Accepted: 12 February 2024

DOI: 10.1111/gcb.17222

Global Change Biology WILEY

RESEARCH ARTICLE

A new empirical framework to quantify the hydraulic effects of soil and atmospheric drivers on plant water status

Maurizio Mencuccini[1,2] | William R. L. Anderegg[3,4] | Oliver Binks[1] | Thorsten Knipfer[5] | Alexandra G. Konings[6] | Kim Novick[7] | Rafael Poyatos[1,8] | Jordi Martínez-Vilalta[1,8]

[1]CREAF, Bellaterra, Spain

[2]ICREA, Barcelona, Spain

[3]Wilkes Center for Climate Science and Policy, University of Utah, Salt Lake City, Utah, USA

[4]School of Biological Sciences, University of Utah, Salt Lake City, Utah, USA

[5]Faculty of Land and Food Systems, The University of British Columbia, Vancouver, British Columbia, Canada

[6]Stanford University, San Francisco, California, USA

[7]University of Indiana, Bloomington, Indiana, USA

[8]UAB, Bellaterra, Spain

Correspondence
Maurizio Mencuccini, CREAF, Bellaterra, Spain.
Email: m.mencuccini@creaf.uab.cat

Funding information
Spanish National Plan for Scientific and Technical Research and Innovation, Grant/Award Number: PID2022-137270NB-I00 and PRE2018-086096; Horizon 2020 Framework Programme, Grant/Award Number: 862221; Natural Sciences and Engineering Research Council of Canada; Alfred P. Sloan Foundation

Abstract

Metrics to quantify regulation of plant water status at the daily as opposed to the seasonal scale do not presently exist. This gap is significant since plants are hypothesised to regulate their water potential not only with respect to slowly changing soil drought but also with respect to faster changes in air vapour pressure deficit (VPD), a variable whose importance for plant physiology is expected to grow because of higher temperatures in the coming decades. We present a metric, the stringency of water potential regulation, that can be employed at the daily scale and quantifies the effects exerted on plants by the separate and combined effect of soil and atmospheric drought. We test our theory using datasets from two experiments where air temperature and VPD were experimentally manipulated. In contrast to existing metrics based on soil drought that can only be applied at the seasonal scale, our metric successfully detects the impact of atmospheric warming on the regulation of plant water status. We show that the thermodynamic effect of VPD on plant water status can be isolated and compared against that exerted by soil drought and the covariation between VPD and soil drought. Furthermore, in three of three cases, VPD accounted for more than 5 MPa of potential effect on leaf water potential. We explore the significance of our findings in the context of potential future applications of this metric from plant to ecosystem scale.

KEYWORDS
homoiohydry, isohydry, soil drought, vapour pressure deficit, water status regulation

1 | INTRODUCTION

Terrestrial plants live along a hydraulic continuum with their water potential bracketed between that of soil water (as high as 0 MPa) and that of atmospheric water vapor (as low as −100 MPa). The water status of terrestrial plants is closely connected to water potential, which is regulated via the control of water loss at the leaf surface and via water supplied by hydraulic transport through roots, stem and leaves given the constraints from soil and atmospheric water availability. Much attention has been paid to developing models describing the regulation of water loss by leaf stomata. By comparison, the regulation of water potential has received less attention (Martínez-Vilalta et al., 2014; Novick et al., 2019), although, in many ways, the regulation of water potential to avoid damaging levels of water stress is complementary to the regulation of water use via stomatal behaviour.

Developing metrics that directly quantify water status regulation (Kannenberg et al., 2022; Knipfer et al., 2020) is important for several reasons. First, microwave remote sensing techniques can quantify variability of canopy water status at several spatial and

temporal scales (Holtzman et al., 2021; Konings et al., 2019, 2021), hence metrics of water status regulation can be useful in aiding the interpretation of this variability. Second, technology is improving for continuous measurement of plant water status in the field (Guo & Ogle, 2019; Novick et al., 2022), presenting novel opportunities for the evaluation of water status regulation at hourly to daily timescales. Third, it is necessary to determine whether traits measured under laboratory conditions relate to metrics of water status regulation in vivo. Physiological traits are expected to be relatively stable over time and relatively independent of changes in environmental conditions. Conversely, field-applicable metrics will often incorporate physiological responses to environmental drivers, as is the case for metrics of water use regulation (e.g., canopy conductance at reference VPD or response of canopy conductance to VPD) (Kannenberg et al., 2022). Consequently, the relationship between traits and field performance can be complex (Mencuccini et al., 2019; Venturas et al., 2021). Using a multi-biome dataset of tree water fluxes, water use metrics were found to be coordinated with leaf and xylem hydraulic traits (Flo et al., 2021).

Several existing metrics aim to quantify the regulation of leaf water potential Ψ_{leaf}. The degree of isohydric/anisohydric control of water potential can be quantified by examining changes in the difference between pre-dawn (Ψ_{pd}) and midday (Ψ_{md}) water potentials $\Delta\Psi=\Psi_{pd}-\Psi_{md}$ (Klein, 2014; Martínez-Vilalta & Garcia-Forner, 2017), stomatal responses to Ψ_{md} (Klein, 2014), the slope σ of the relationship between Ψ_{pd} and Ψ_{md} (Martínez-Vilalta et al., 2014) and the hydroscape area, that is, the area included between the boundary line of the cloud of Ψ_{pd}–Ψ_{md} pairs and the 1:1 line (Meinzer et al., 2016). These metrics of isohydry, also referred to as metrics of regulation stringency (e.g., Meinzer et al., 2016), were also found to relate with traits, that is, leaf turgor loss point, vulnerability to cavitation and several other functional proxies (Martínez-Vilalta et al., 2014).

Current metrics of isohydry have limitations (Feng et al., 2019; Kannenberg et al., 2022; Knipfer et al., 2020). First, because they only examine the relationship between pre-dawn and midday water potentials, $\Delta\Psi$, σ and the hydroscape area are essentially undefined at the daily time scale. Since these isohydry metrics are undefined at the daily time scale, we use the wider term of water potential regulation, to encompass both daily and seasonal time scales, throughout this paper. Additionally, the second of the two direct external drivers of plant water potential, that is, VPD, atmospheric vapor pressure deficit is not considered (Novick et al., 2019; Tardieu & Simonneau, 1998). This is relevant, given current trends of increasing air temperatures and the likelihood that higher VPD will lead, directly or indirectly, to more negative water potentials in many ecosystems (Grossiord et al., 2020). The $\Delta\Psi$ metric is applicable at the daily time scale, but its relationship to the external effects caused by VPD remains unquantified. Finally, the σ isohydry metric (Martínez-Vilalta et al., 2014) has been criticized on the ground that it confounds plant traits with other environmental effects (Feng et al., 2019), leading to a suggestion that the isohydric/anisohydric framework should be abandoned (Hochberg et al., 2018).

Our aim here is to develop a water potential stringency metric S^{ws} that (a) quantifies the effects of both VPD and Ψ_{soil} and (b) can be applied at daily and seasonal time scales. This paper shows that this is possible by (c) quantifying the departure of observed water potential from the predictions of a model representing both thermodynamic forces (i.e. both soil and atmospheric drought) when no physiological regulation (no stomatal limitations for a given hydraulic supply) occurs. Using data collected in two field experiments as case studies, we ask the following questions: (1) to what extent is S^{ws} sensitive to differences in Ψ_{leaf} regulation in response to experimental treatments including VPD manipulations? (2) How does its sensitivity compare against other common metrics, such as σ, $\Delta\Psi$ and the hydroscape area? (3) How does the regulation of Ψ_{leaf} under high VPD compare to the regulation under negative Ψ_{soil}? We further examine whether the accuracy of S^{ws} calculation is sensitive to observational record length.

2 | MATERIALS AND METHODS

2.1 | Regulation of leaf water potential

We derive a null model for the hydraulic effects exerted on Ψ_{leaf} by VPD and Ψ_{soil}, such that the internal regulation of plant water potential can be examined. We start by assuming steady-state flow in plants, i.e., transpiration equals plant water transport. Given that most time series of Ψ_{leaf} only include midday measurements, we limit the analysis to the case of $\Psi_{leaf}=\Psi_{md}$. However, the concept presented here can be expanded to full diurnal time courses of Ψ_{leaf}, or to non-transpiring leaves (approximating stem Ψ). The original derivation for this steady-state water balance between supply and demand assumed well-coupled canopies (Whitehead & Jarvis, 1981):

$$\Psi_{md} = \Psi_{pd} - \frac{g_{tot}}{k_L}\mathrm{VPD}. \quad (1)$$

In Equation (1), g_{tot} (leaf vapor conductance, sum of stomatal and boundary layer conductances) and k_L (whole-plant hydraulic conductance divided by leaf area, assuming $\Psi_{pd}=\Psi_{soil}$, cf., Section 4) are dependent on plant water potential, but the exact form of this dependency is not relevant here. This formulation omits gravity-induced head-losses to the soil-to-leaf gradient since they cancel out in Equation (5). In Equation (1), VPD is vapor pressure deficit outside of the leaf boundary layer (i.e., assuming leaves are equilibrated at air temperature). This equilibrium assumption is justified because leaf-to-air VPD and VPD of the air are generally strongly correlated. The assumption can be relaxed in future studies if continuous observations of leaf canopy temperature are available, but we recognize that the relevant VPD for the plants may be higher than the VPD of the air. Assuming that time series are available for Ψ_{md}, Ψ_{pd} and VPD, we calculate the following ratio for each point i in the time series:

$$\left(\frac{g_{tot}}{k_L}\right)_i = \frac{\Psi_{pd,i} - \Psi_{md,i}}{VPD_i}, \quad (2)$$

where the quantity $\left(\frac{g_{tot}}{k_L}\right)_i$ stands for the value of the ratio of the two properties at time i. The $\left(\frac{g_{tot}}{k_L}\right)_i$ indexes the variability over time of leaf conductance per unit of leaf-specific hydraulic supply capacity. As part of the calculation of a null model, it is necessary to define a proxy for the maximum value of this quantity. A suitable benchmark is:

$$\widehat{\frac{g_{tot}}{k_L}} = \text{quantile}, 99\left(\text{pdf}\left(\left(\frac{g_{tot}}{k_L}\right)_i\right)\right). \quad (3)$$

Since $\left(\frac{g_{tot}}{k_L}\right)_i$ increases with Ψ_{pd} (where $\Psi_{pd} < 0$) and decreases with VPD, the 99th quantile provides a reference value for the maximum value of the distribution of leaf conductance per unit of leaf-specific water supply under well-watered conditions. Using the 99th percentile rather than the absolute maximum reduces the impact of measurement noise. Alternative calculations using the 95th percentile are presented in Data S1 and gave similar results. Taking the ratio of stomatal to hydraulic conductance accounts for the fact that g_{tot} and k_L co-vary depending on species and time. The reference ratio $\widehat{\frac{g_{tot}}{k_L}}$ can be defined in alternative ways, for example, at fixed values of VPD and Ψ_{pd} as opposed to by reference to the empirical distribution, to standardize across case studies. The impacts of these alternative definitions on measures of stringency are discussed later. We then define the hydraulic effects of the environment on leaf water potential Ψ_{hf} (MPa, subscript hf for hydraulic 'forcing') at time i:

$$\Psi_{hf,i} = \Psi_{pd,i} - \widehat{\frac{g_{tot}}{k_L}} VPD_i. \quad (4)$$

Equation (4) is identical to Equation (1) but the ratio $\widehat{\frac{g_{tot}}{k_L}}$ remains at the reference well-watered value. Because Ψ_{pd} and VPD now vary over time, Equation (4) provides a null model of how plant water potential changes if internal conductances are not regulated (cf., Section 4, as to how an expression containing Ψ_{pd} may differ from an expression containing Ψ_{soil}). This null model represents a time-dependent metric of environmental effects (the 'forcing') that combines both VPD and soil water limitation, because the conversion of VPD on the thermodynamic scale can use individual-specific information on the sensitivity to the environment. Referencing these effects to the maximum value of leaf conductance per unit of leaf-specific supply capacity quantifies the thermodynamic sensitivity to keeping stomata open and maintaining water supply, given increases in VPD and/or declines in Ψ_{pd}. Plant regulation acts against these effects (Figure 1).

The null model of Equation (4) can be employed to assess the degree of regulation of water potential by comparing the measured Ψ_{leaf} against the corresponding Ψ_{hf} under the same conditions (i.e., same VPD and Ψ_{pd}). We define the stringency of water potential regulation (MPa) as the departure from the effects of Ψ_{pd} and VPD:

$$S_i^{ws} = \Psi_{md,i} - \Psi_{hf,i} = VPD_i\left(\widehat{\frac{g_{tot}}{k_L}} - \left(\frac{g_{tot}}{k_L}\right)_i\right). \quad (5)$$

While Equation (1) is based on a steady-state model of water transport (demand = supply), changes in S^{ws} can reflect non-steady-state changes in the ratios of vapor to hydraulic conductance via their effects on Ψ_{md}. When $S^{ws} = 0$, the ratio of vapor to hydraulic conductance is identical to the ratio under well-watered conditions and $\Psi_{md} = \Psi_{hf}$. Instead, $S^{ws} > 0$ when $\frac{g_{tot}}{k_L}$ is low relative to $\widehat{\frac{g_{tot}}{k_L}}$, in which case $\Psi_{md} > \Psi_{hf}$. The environmental effects on plant water potential are isolated in Ψ_{hf}, and the difference $S^{ws} = \Psi_{md} - \Psi_{hf}$ represents the plant-driven component of the regulation in leaf water potentials (Figure 1).

Because Equation (4) is additive, the total effect on Ψ_{md} can be decomposed into the effect by VPD alone (i.e., $\Psi_{hf,VPD}$), Ψ_{pd} alone (i.e., $\Psi_{hf,\Psi_{pd}}$) and the seasonal covariation between VPD and Ψ_{pd} (i.e., $\Psi_{hf,cov}$). Equally, one can separate the proportion of plant water potential regulation, for VPD (i.e., S_{VPD}), Ψ_{pd} (i.e., $S_{\Psi_{pd}}$) and their covariation (i.e., S_{cov}) (see Data S1 for derivations). Beyond the study of how stringency changes over time, this new framework can be employed to also examine two properties calculated across the entire time series, that is, the regression slope between Ψ_{md} and Ψ_{hf} (equivalent to σ of (Martínez-Vilalta et al., 2014)) and the area encompassing all pairs of Ψ_{md} and Ψ_{hf} points (equivalent to hydroscape area of (Meinzer et al., 2016)). Beyond σ and hydroscape area, we also compare our metric against DY.

2.2 | Empirical tests

We employ two experimental datasets to test whether S^{ws} provides a sensitive metric of the daily stringency of Ψ_{md} regulation. The first dataset comes from the SUMO experiment conducted in New Mexico described in (Sevanto et al., 2018a, 2018b). The Los Alamos Survival–Mortality experiment (SUMO) was located on Frijoles Mesa near Los Alamos, New Mexico, USA. This was a multi-year-long tree manipulation study that investigated the relative impacts of drought and warming on plant function in a semi-arid region. The study examined the effects of drought and heat treatments in isolation and in combination with a crossed design. The experiment was in a piñon-juniper (*Pinus edulis* Engelm.–*Juniperus monosperma* (Engelm.) Sarg.) woodland near the ponderosa pine (*Pinus ponderosa* Dougl.) forest ecotone. The water potential data (pre-dawn and midday) as well as the time series of VPD were downloaded from https://ess-dive.lbl.gov/. Because empirical RH data from within the chambers are not publicly available, VPD values inside the heated chambers were obtained using an empirical regression of mean monthly VPD values based on Figure S1 from (Grossiord, Sevanto, Dawson, et al., 2017).

The second dataset comes from an experiment manipulating air temperature and water supply of forest red gum (*Eucalyptus tereticornis* Sm.) trees inside 12 whole-tree climate-controlled chambers (WTC) in Australia (Aspinwall et al., 2016; Drake et al., 2016). The WTCs are large, approximately cylindrical structures topped with a cone that enclose a single tree rooted in the soil underneath. Six chambers tracked ambient temperature and six chambers tracked

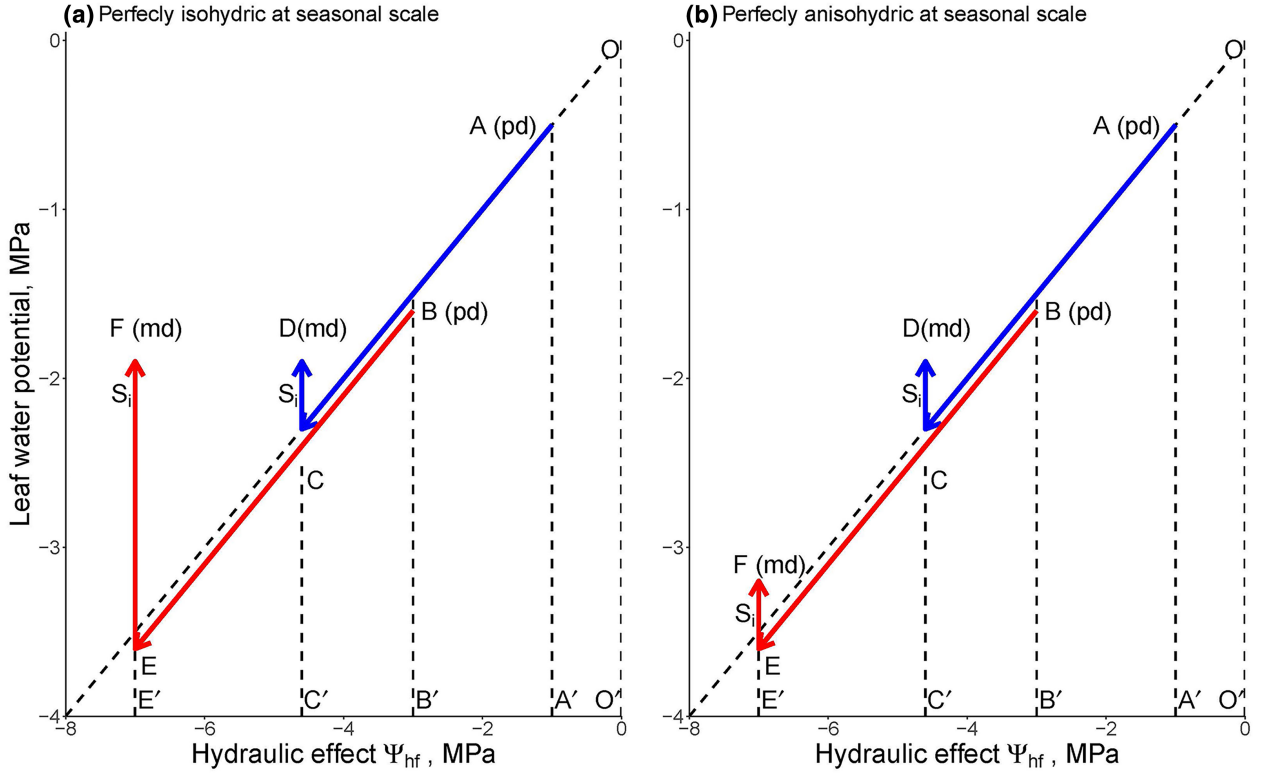

FIGURE 1 Conceptual diagram of the relationships between leaf water potential Ψ_{leaf}, measured at either predawn (pd) or midday (md) and the combined hydraulic effects caused by Ψ_{soil} plus VPD (Ψ_{hf}). For both panels, blue line, springtime day, close-to-zero Ψ_{pd}; red line, summertime day, negative Ψ_{pd}. At springtime, the effect of Ψ_{soil} (assumed equal to Ψ_{pd}) equals $\overline{A'O'}$ and the effect of VPD equals $\overline{C'A'}$. At summertime, the effect of Ψ_{soil} equals $\overline{B'O'}$ and the effect of VPD equals $\overline{E'B'}$, respectively. In both days, the observed Ψ_{md} is less negative than the total hydraulic effect predicted based by Ψ_{hf} (compare D with C and F with E). The vertical segments $\overline{DC}$ with $\overline{FE}$ give the regulation S_i against VPD, while $-\Delta\Psi = \Psi_{md} - \Psi_{pd}$ is the regulation against VPD that the plant did not do. (a), Left-hand panel, a perfectly isohydric plant (at the seasonal time scale) in which Ψ_{md} remains constant through the season despite changes in the two drivers (compare Ψ_{leaf} at D with F); (b), right-hand panel, a perfectly anisohydric plant in which stringency of regulation remains constant despite changes in the two drivers (compare $\overline{DC}$ with $\overline{FE}$). Note that the hydraulic effect caused by VPD for the two plants depends on plant-specific values of $\frac{\widehat{g_{tot}}}{k_L}$ and therefore likely to change between the two idealised cases, but this is not represented in the figure. Beside the two cases presented here, other scenarios are possible, depending on the balance between regulation against VPD and Ψ_{pd}.

ambient temperature +3°C warming in a 2-year-long experiment. Relative humidity RH in the warmed treatment was controlled to match the RH observed in the ambient treatment (about 62% during daylight hours), which meant that VPD was higher in the warmed compared to the ambient chambers (by between 0.3 and 1.0 kPa at midday compared to control). A water exclusion treatment was added to half of the trees on 12 February 2014, whereby trees were irrigated regularly every 15 days with half the mean monthly rainfall, leading to small changes in Ψ_{pd} in the second part of the experiment. We employ here only the data from the second year of the experiment. Data were downloaded from: https://figshare.com/articles/dataset/Drake_NewPhyt_2016_WTC3_RtoGPP_forfigshare_zip/3122104/1.

2.3 | Statistics

To address question (1) (to test the sensitivity of the metric to experimental treatments), we fit linear mixed models to the two datasets to examine whether daily Ψ_{hf} and regulation stringency S^{ws} vary across treatments and species (SUMO) or treatment combinations (Australia). To address question (2) (to compare against existing seasonal metrics), we first fit the same mixed models to Ψ_{md} as a function of Ψ_{pd} and treatment to obtain σ (Martínez-Vilalta et al., 2014), and to $\Delta\Psi$ as a function of treatment (Klein, 2014). Using the SUMO experiment as a test case, we also calculate the hydroscape area A_{HS} (Meinzer et al., 2016) and compare it against the equivalent stringency areas (i.e., A_s) across species and treatments. We define the hydroscape area as the triangular area within the boundary line of the point distribution, the 1:1 line and the vertical line at $\Psi_{pd} = 0$. To obtain the boundary line, we employ quantile regression in quantreg (Koenker, 2005) in R (R Development Core Team, 2013) using the command rq and the 5% quantile of the regression between Ψ_{md} and Ψ_{pd}. We then integrate geometrically. To calculate the stringency areas, we first employ quantile regression as above with the 95% quantile of the Ψ_{hf}–Ψ_{md} regression to get the upper boundary of the point distribution. We then integrate geometrically between this line and the 1:1 line down to the minimum recorded Ψ_{hf} for each species/

treatment combination (cf., Figure 3 as an example). All areas are calculated separately for each individual tree and the means and 95% confidence intervals for each species/treatment combination are estimated across individuals. To address question (3) (to test the relative regulation against VPD and Ψ_{soil}), we quantify the relative importance of the effects caused by VPD and Ψ_{pd}, as well as the regulation against these drivers, by plotting these variables against the total effect. In all cases we use tree (SUMO) and chamber (WTC experiment) as random intercepts and the applied treatments as fixed factors.

To assess the impact of sample size on the accuracy of the variables related to regulation stringency, we use the SUMO dataset, because its large size permits sub-sampling. We obtain estimates of the ratio $\widehat{\frac{g_{tot}}{k_L}}$, the total hydraulic effect Ψ_{hf}, regulation stringency S^{ws} and the proportion of regulation attributable to VPD in the complete dataset and in random sub-samples including $N = 5$, 10, 20, 50, 100, 200, 400 and 600 measurements, using both the 95th and the 99th percentile of the distribution of $\widehat{\frac{g_{tot}}{k_L}}$. Computations are repeated 1000 times per species and treatment combinations using different random sub-samples (with replacement) calculated for each individual tree. The distribution of the variability in the results therefore reflects the sum of the uncertainty of the estimates for each tree (i.e., the length of the time series) plus the variability across individuals. To assess the impacts of using definitions of the reference ratio $\widehat{\frac{g_{tot}}{k_L}}$ alternative to Equation (3) on the calculated measures of stringency, we use multiple regressions of $\left(\frac{g_{tot}}{k_L}\right)_i$ against VPD and Ψ_{pd} to estimate $\widehat{\frac{g_{tot}}{k_L}}$ at VPD = 0.1 or 0.5 kPa and $\Psi_{pd} = -0.1$ or −0.5 MPa for each species-treatment combination.

3 | RESULTS

Of all the water status metrics, only the stringency metric (e.g., S^{ws}) was able to discern treatment effects in these two experiments. A highly significant relationship between Ψ_{md} and Ψ_{pd} was found in the SUMO experiment for both *P. edulis* and *J. monosperma* (both $p < .0001$, Figure 2 top). However, a treatment effect was not found in either species or for the two species combined (Table 1A). Ψ_{md} was also significantly related to Ψ_{pd} in the *E. tereticornis* experiment, but again no significant effect of the applied treatments was found (Table 2A; Figure 2 bottom). Similar results were obtained for $\Delta\Psi$, the water potential difference between pre-dawn and midday (Tables 1B and 2B) and for hydroscape area A_{HS} (Table 1E; note that A_{HS} could not be calculated for some treatments in the *E. tereticornis* experiment). Ψ_{md} was highly significantly and linearly related to total hydraulic effect Ψ_{hf} in all three species (at least $p < .0001$, Tables 1C and 2C; Figure 3), although the best model (as assessed using a delta AIC metric) was that of a concave-up quadratic regression between Ψ_{md} and Ψ_{hf} (AIC always smaller by at least 2 units for the quadratic regressions). In contrast to the previous metrics, treatment effects for Ψ_{md} against Ψ_{hf} were found in *J. monosperma*, when the two species at SUMO were combined and for *E. tereticornis* (Table 1C). Treatment effects on total regulation S^{ws} were also found in *J. monosperma*, for the two species combined at SUMO and for *E. tereticornis* (data not given, since results for treatment are identical to those given above against Ψ_{hf}).

Consistent with these results, a significant relationship was found between the slopes of the Ψ_{hf}–Ψ_{md} relationships and the slopes σ of the Ψ_{pd}–Ψ_{md} relationships (Martínez-Vilalta et al., 2014) but the confidence intervals were generally larger for the second (Figure S1). Across both species at SUMO and all treatments, the hydroscape area A_{HS} showed a broad inverse relationship with the equivalent area of stringency (Figure 4), with larger areas indicating a stricter water potential regulation. However, stringency areas had often smaller standard errors compared to A_{HS} and showed significantly larger values in Heat and Heat+Drought relative to Ambient in the analysis combining both species ($p < .00001$) and in *P. edulis* ($p < .00001$), but not in *J. monosperma*. No such differences were apparent with A_{HS} (always $p > .05$, cf., Table 1D,E).

Total hydraulic effect Ψ_{hf} occasionally reached values down to −12.6 MPa in *J. monosperma* (−7.9 MPa in *P. edulis*), with Ψ_{md} reaching a minimum of −9.6 MPa (−4.2 MPa in *P. edulis*). The 5% quantiles of Ψ_{hf} (i.e., a more robust estimate of the minimum of the distribution of Ψ_{hf}) reached −9.8 and −8.6 MPa for juniper and piñon pine, respectively, and varied significantly with species and treatment (both $p < .0001$). In both species, Heat and Heat+Drought were the treatments with the most negative values of Ψ_{hf}. At the opposite extreme, Ψ_{hf} remained mostly above −5 MPa in *E. tereticornis*. Seasonal covariation between VPD and Ψ_{pd} in *J. monosperma* accounted for a significant proportion of the total effect on Ψ_{hf}. Conversely, the covariation effect was not significant in *P. edulis* and the slopes of the linear regressions between VPD and Ψ_{pd} were never different from zero (Figure 5).

The mean net effect of VPD was −5.4 MPa (95% quantile, −8.7 MPa) in *P. edulis* and −5.2 MPa (95% quantile, −10.0 MPa) in *J. monosperma* ($p < .00001$ for the difference across species), a result of species-specific differences in $\widehat{\frac{g_{tot}}{k_L}}$. The proportion of the total effect Ψ_{hf} caused by VPD increased in *P. edulis* but decreased in *J. monosperma* at more negative Ψ_{hf} ($p < .0001$ for both species) (Figure 5 top), a consequence of the different behaviour of Ψ_{pd} in the two species. The slope of the effect by VPD as a function of Ψ_{hf} did not vary significantly across treatments in either *J. monosperma* ($p = .99$) or *P. edulis* ($p = .57$, Figure 5 top). Conversely, the absolute effect of VPD was significantly more negative, as expected, for Heat and Heat+Drought relative to Ambient (21% and 27%, respectively). Interestingly however, these results were obtained only when Ψ_{hf} was calculated 'globally,' using either the pooled $\widehat{\frac{g_{tot}}{k_L}}$ by species, the values of $\widehat{\frac{g_{tot}}{k_L}}$ for the Ambient treatment as a reference, or by extrapolating $\widehat{\frac{g_{tot}}{k_L}}$ to reference values using a multiple regression against VPD and Ψ_{pd} for all treatments pooled. When $\widehat{\frac{g_{tot}}{k_L}}$ was calculated instead for each tree separately, the effect of VPD did not vary by treatment ($p = .21$). The results for *E. tereticornis* resembled those for *P. edulis*, although here the net effect of VPD could be as low as −4.7 MPa. The proportion of Ψ_{hf} caused by VPD also increased with Ψ_{hf} in *E. Tereticornis*, although the effect by VPD remained high throughout and in all treatments (Figure 4 bottom).

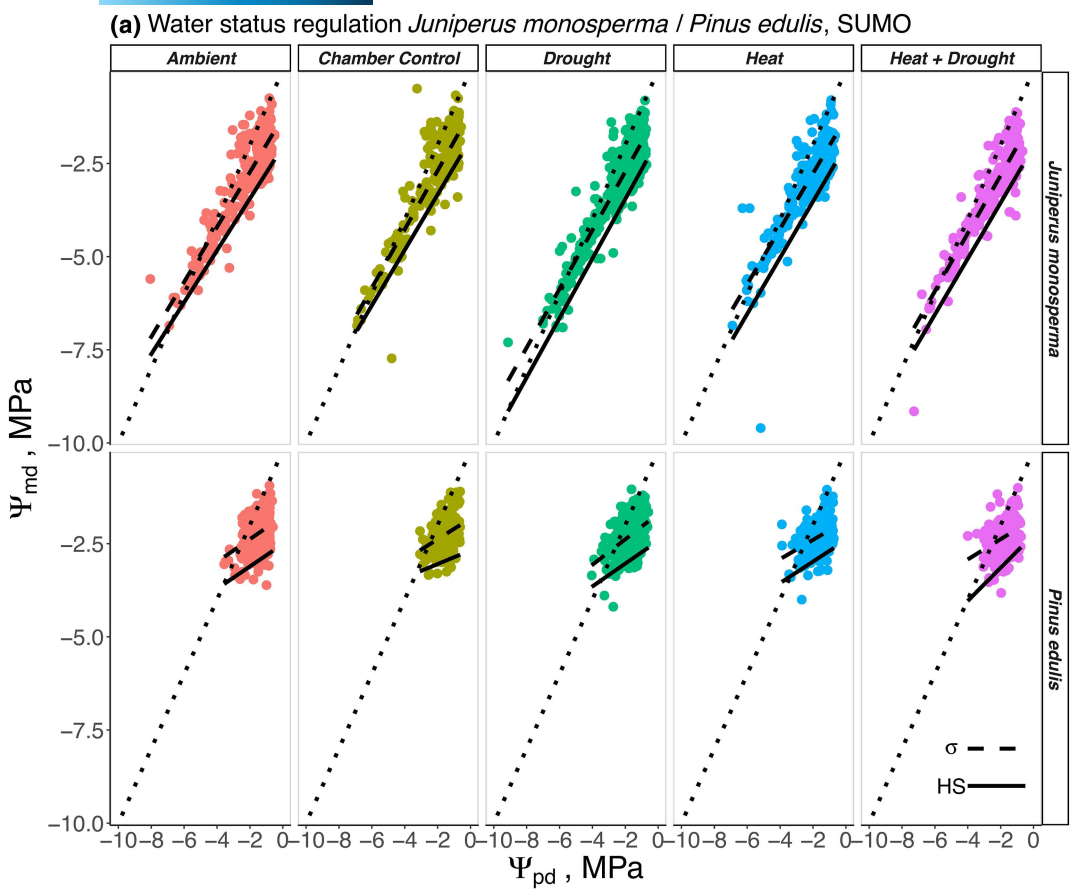

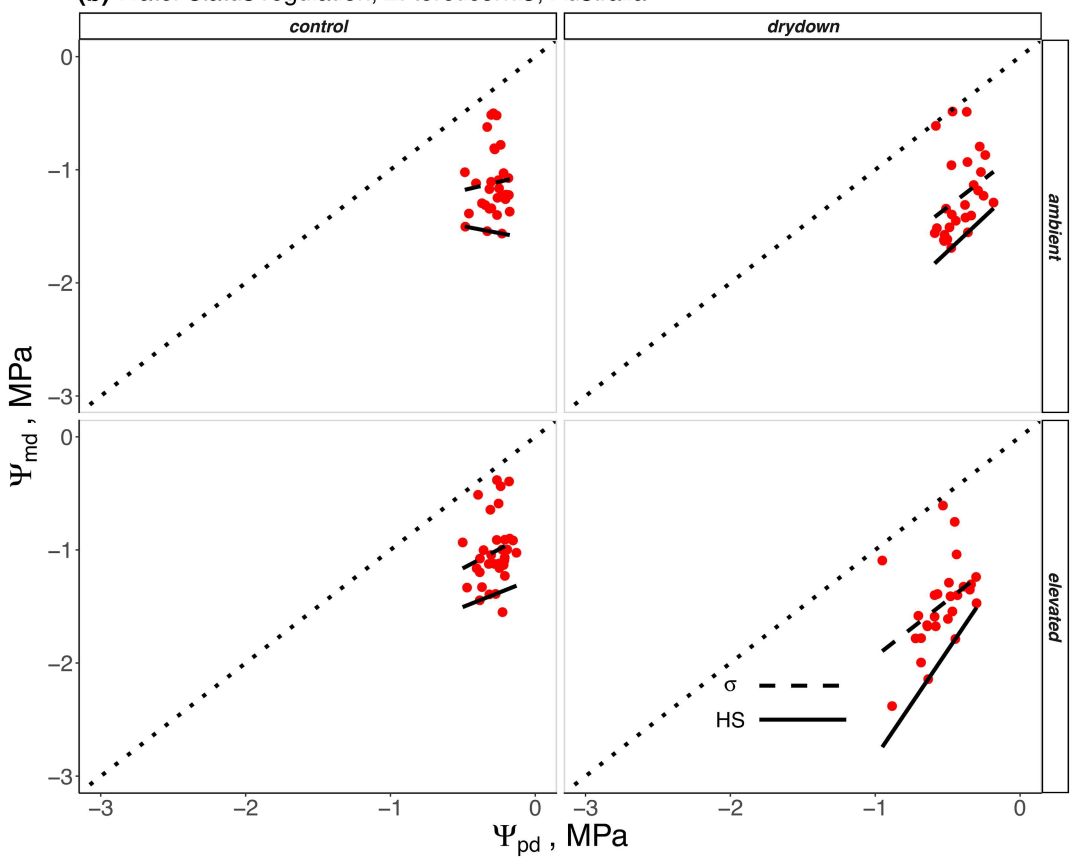

FIGURE 2 Plots of midday Ψ_{md} against predawn leaf water potential Ψ_{pd}, for (a) the SUMO (top) and (b) the Australian WTC experiment (bottom). Plots are given separately by species and treatment (top) and treatment combinations (bottom). Continuous regression lines mark the lower 5% quantile used to calculate the hydroscape area; dashed regression lines give the estimate of slope σ from Martínez-Vilalta et al. (2014). The dotted line is the 1:1 line. Note that the slopes of the continuous lines for both drydown treatments in the Australian experiment are so steep that hydroscape area cannot be calculated.

With $\widehat{\frac{g_{tot}}{k_L}}$ calculated 'globally' (i.e., across all treatments and individuals), total regulation was less stringent and had a lower slope as a function of Ψ_{hf} in *J. monosperma* (Figure 6, dark grey points, both $p < .00001$). Regulation was 40%–48% more stringent in *P. edulis* (36%–37% in *J. monosperma*) in Heat and 47%–57% (42%–43%) in Heat+Drought relative to Ambient ($p < .00001$ for both species), respectively, depending on how $\widehat{\frac{g_{tot}}{k_L}}$ was calculated. The maximum values of regulation (calculated as the 95% quantile of the distributions by individual) also varied significantly as a function of species and treatment, again with higher values for Heat and Heat+Drought relative to Ambient ($p < .00001$), reaching values of ~6.4 MPa for piñon pine in those treatments. Very similar results were obtained for regulation against VPD S_{VPD} (coloured points, Figure 6). S_{VPD} was significantly higher (more positive values, $p < .00001$) and it tightly increased at negative Ψ_{hf} in *P. edulis* ($R^2_m = 0.51$), whereas it broadly decreased ($R^2_m = 0.19$) and had generally negative values in *J. monosperma*. Again, stringency S_{VPD} was significantly higher ($p < .00001$, Figure 6) in Heat and Heat+Drought, despite the higher values of Ψ_{hf}, relative to Ambient in both species.

Because these results depended on how $\widehat{\frac{g_{tot}}{k_L}}$ was calculated, we explored how $\widehat{\frac{g_{tot}}{k_L}}$ varied across all treatments. The 99% quantiles of $\widehat{\frac{g_{tot}}{k_L}}$ calculated by individual were significantly lower in Drought, Heat, and Heat+Drought relative to ambient ($p < .001$ and $p < .10$ in *P. edulis* and *J. monosperma*, respectively, cf., Figure S2 for the overall distributions). This was expected, given generally lower leaf conductance under high VPD and soil drought treatments. To compare reference values under identical environmental conditions, we used multiple regressions to extrapolate $\widehat{\frac{g_{tot}}{k_L}}$ for each tree at reference values of VPD = 0.1 or 0.5 kPa and $\Psi_{pd} = -0.1$ or −0.5 MPa. These extrapolated values significantly varied by treatment in *P. edulis* ($p < .001$), again being lower in Drought, Heat, and Heat+Drought, but not in *J. monosperma* ($p = .23$), with a significant interaction between species and treatment ($p < .001$).

The accuracy and precision in the estimation of regulation stringency depended on several factors. The ratio $\widehat{\frac{g_{tot}}{k_L}}$ determined for each species/treatment combination varied both within as well as across individuals, although a proportion of this variability was due to sampling dates during extreme drought periods when $\Psi_{pd} < \Psi_{md}$, giving rise to negative ratios (Figure S2) (Plaut et al., 2012). To avoid affecting the estimate of the 99% quantile of the $\widehat{\frac{g_{tot}}{k_L}}$ distribution, we filtered out these dates. The accuracy of all regulation variables depended on the sample size employed to obtain $\widehat{\frac{g_{tot}}{k_L}}$ for each time series. In general, sample sizes of $n \leq 50$ (i.e., length of time series x number of individuals per treatment) resulted in biased and more uncertain estimates of the absolute and relative effects caused by VPD (Figures S3–S6). Estimates of the total effects on Ψ_{md} obtained from the multiple regression estimating $\widehat{\frac{g_{tot}}{k_L}}$ at VPD = 0.1 kPa and $\Psi_{soil} = -0.1$ MPa were closely related to estimates obtained using $\widehat{\frac{g_{tot}}{k_L}}$ from Equation (3) (Figure S7). Despite these close relationships, systematic differences were evident for both species. Using reference values of VPD = 0.5 kPa and $\Psi_{pd} = -0.5$ MPa slightly increased the biases for *J. monosperma* but decreased them for *P. edulis* (data not shown). A similar picture was found for correlations and biases in estimates of regulation stringency S^{ws} (Figure S8). Using the 95th percentile as opposed to the 99th percentile of the distribution of Ψ_{hf} always gave lower estimates of total hydraulic effect Ψ_{hf}, mean net effect of VPD, proportion of the total effect caused by VPD on Ψ_{md} and total regulation S^{ws} (Figures S4–S6).

4 | DISCUSSION

4.1 | The significance of our findings

Our approach has precedence in the ecological literature on animal homoiothermy, where the concept of 'operative environmental temperature,' calculated via equations of steady-state energy balance, has been in use since the 1970s as a reference null model against which to assess measured body temperature (Bakken et al., 1985). The hydraulic quantity Ψ_{hf} puts on the same scale the two environmental drivers of plant water potential, i.e., the potentials of soil and atmospheric water. Temperature and atmospheric pressure are also known to directly affect plant water potentials (Tyree & Jarvis, 1982); however, their effects are comparatively smaller. Air temperature, radiation, [CO_2], and other site properties also affect plant water status via stomatal conductance and photosynthesis or via whole-plant conductance. We contend that the primary reason for the ongoing debate over the interpretation and value of isohydry indices lies in the failure to separate the direct drivers of VPD and Ψ_{soil} (here achieved via a suitable null model of plant water status), rather than in the failure to account for indirect environmental effects on plant gas exchange or liquid water transport (Novick et al., 2019).

In our analysis, we quantify the magnitude of the changes in leaf water potential relative to the changes that would occur if no internal regulation of the liquid-phase and vapor-phase conductances took place. In essence, our approach provides a null model based on environmental drivers, against which internal regulation is assessed. Therefore, the S^{ws} metric quantifies the direction and magnitude of the internal regulation of water status under specific sets of external conditions. Over time, water status varies strongly in response to both stomatal and photosynthetic signals as well as VPD changes (Anderegg et al., 2017). This dependency on VPD is captured in both semi-empirical (Rogers et al., 2014) and optimality (Lin et al., 2015; Prentice et al., 2014; Sperry et al., 2017) models of stomatal behavior.

TABLE 1 Results from the whole-tree chamber *Pinus edulis/Juniperus monosperma* experiment. Statistics of the linear models used to detect the effects of (A) Ψ_{pd} and treatment on Ψ_{md} ($R^2_m = 0.16 / 0.82 / 0.78$), (B) treatment on $\Delta\Psi$ ($R^2_m = 0.52 / 0.31 / 0.40$), (C) Ψ_{hf} and treatment on Ψ_{md} ($R^2_m = 0.07 / 0.80 / 0.71$), (D) treatment on A_s ($R^2_m = 0.75 / 0.03 / 0.50$), and (E) treatment on A_{Hs} ($R^2_m = 0 / 0.02 / 0.39$). Multiple R^2 values for each case refer to *P. edulis*, *J. monosperma* or the two species combined. Sample size $n = 1462/1512$ for *P. edulis/J. monosperma*, for tests (A) to (C); Samples size $n = 25/27$ for *P. edulis/J. monosperma* for tests (D) and (E); Appr. df, approximate number of degrees of freedom; *, $p < .05$; **, $p < .01$; ***, at least $p < .001$. Results are from the ANOVA table of the mixed effect models using individual tree as the random factor. Interactions are included only when variance inflation factors <5 and model AIC is lower.

	Pinus edulis			*Juniperus monosperma*			Combined		
Variable	***F*-test**	**Appr. df**	***p*-value**	***F*-test**	**Appr. df**	***p*-value**	***F*-test**	**Appr. df**	***p*-value**
(A) Ψ_{md}									
Ψ_{pd}	263.8	(11, 446)	<.00001***	6507.8	(11, 504)	<.00001***	2111	(12, 856)	<.00001***
Treatment	0.19	(4, 25)	.94	1.39	(4, 27)	.26	0.89	(4, 55)	.48
Species							297	(1, 71)	<.00001***
Species* Ψ_{pd}							425	(12, 887)	<.00001***
(B) $\Delta\Psi$									
Treatment	0.19	(4, 25)	.94	1.4	(4, 27)	.26	0.89	(4, 55)	.48
Species							155	(1784)	<.00001***
Species* Ψ_{hf}							425	(12, 887)	<.00001***
(C) Ψ_{md}									
Ψ_{hf}	101.4	(11419)	<.00001***	6015	(11472)	<.00001***	2401	(12900)	<.00001***
Treatment	2.0	(4, 25)	.12	3.8	(4, 27)	<.00001***	3.9	(4, 56)	.002**
Species							478	(1640)	<.00001***
Species* Ψ_{hf}							1167	(12900)	<.00001***
(D) A_s									
Treatment	22.6	(4, 25)	<.00001***	1.21	(4, 27)	.33	10.2	(4, 52)	<.00001***
Species							29.8	(1, 52)	<.00001***
Species* Treatment							1.7	(1, 52)	.16
(E) A_{HS}									
Treatment	0.10	(4, 25)	.98	1.2	(4, 27)	.34	0.30	(4, 52)	.30
Species							39.16	(1, 52)	<.00001***
Species* Treatment							0.79	(1, 52)	.54

Previous analyses identified water relations (e.g., turgor loss point, Fu & Meinzer, 2019; Meinzer et al., 2016) and hydraulic (xylem vulnerability, for example, (Martínez-Vilalta et al., 2014)) traits as the main correlates of the degree of an/isohydric behaviour, using the hydroscape area and σ, respectively. However, prior empirical analyses did not examine the consequences of regulation against VPD at the daily time scale. This is relevant, since additional variables (e.g., hydraulic capacitance, nighttime hydraulic balance, carbohydrate dynamics) and processes (temperature regulation, internal clocks) may play a role at the daily time scale. Therefore, our finding that the potential 'forcing' of VPD can amount to several MPa is indeed of interest. (Guo et al., 2019) examined the relationships between Ψ_{soil} and VPD but did not employ a generalizable metric like the stringency metric proposed here. A 'baseline' relationship between VPD and stem Ψ_{md} (i.e., the Ψ of a non-transpiring leaf) was developed by (Shackel, 2011) for irrigation management (Shackel et al., 2021), but its application is confined to non-limiting soil water supply.

In response to question (1) (cf., Section 1), we show that our metrics behave more sensitively than earlier metrics, as predicted, across two case studies where VPD levels were manipulated. The interest here is that soil and atmospheric contributions to regulation stringency are examined on the same thermodynamic scale, by examining their effects on plant water status. Previously, this could be done only indirectly, by examining the relative consequences of the changes in the two drivers on stomatal conductance, transpiration, and photosynthesis. This is not entirely satisfactory, given that even at steady state, plant water status depends also on the regulation of whole-plant conductance (i.e., Equation 1) (Martínez-Vilalta et al., 2014; Mencuccini et al., 2019; Whitehead & Jarvis, 1981). Both root and leaf extra-xylary conductance are known to respond to changes in, for example, temperature and radiation (Ehlert et al., 2009; Scoffoni et al., 2015) and to show entrained circadian rhythms (Caldeira et al., 2014).

The focus of plant physiologists has often been in understanding the mechanisms leading to the regulation of leaf water fluxes and status ('trait syndrome' and 'response metrics' approaches, cf.; Kannenberg et al., 2022). This focus on measuring fluxes and traits is not employed here, in favour of developing metrics that instead take advantage of the large data streams of relevant drivers available from, for example, remote sensing or field monitoring of plant water status. Hence, S^{ws} (like σ or A_{HS}) should not be construed as substitutes for the quantification of physiological traits, but as metrics useful to interpret their time series. Because current techniques allow monitoring plant water status (both water content and potential) at tree-to-pixel scales with increasing temporal resolution (Novick et al., 2022), the metrics developed here may also have applications at larger scales, by inverting the problem to isolate the dynamics of water status stringency. Having said that, the approach developed here is based on the composite trait $\widehat{\frac{g_{tot}}{k_L}}$, i.e., the maximum ratio of leaf conductance to leaf-specific hydraulic conductance, albeit we recognize that vapor conductance as defined here includes the boundary layer. Note that this is not the case for either the hydroscape area or σ, both of which incorporate VPD effects. The $\widehat{\frac{g_{tot}}{k_L}}$ is closely related to the intercept Λ of (Martínez-Vilalta et al., 2014) analysis. However, Λ also incorporates a VPD effect (cf., Equation 3 in Martínez-Vilalta et al., 2014).

TABLE 2 Results from the whole-tree chamber *Eucalyptus tereticornis* experiment. Statistics of the linear models used to detect the effects of (A) Ψ_{pd} and treatment on Ψ_{md} ($R^2_m = 0.21$), (B) treatment on $\Delta\Psi$ ($R^2_m = 0.03$), (C) Ψ_{hf} and treatment on Ψ_{md} ($R^2_m = 0.44$) and (D) treatment on S^{WS} ($R^2_m = 0.30$). Sample size $n = 79$, for all tests; df, degrees of freedom; $^{\xi}p < .10$; $^{*}p < .05$; $^{**}p < .01$; $^{***}p < .001$. Results are from the ANOVA table of the mixed effect models using individual chamber as the random factor. Interactions are included only when variance inflation factors are below 5. Statistics on A_{Hs} and A_s could not be calculated because of the low number of points per individual chamber.

Variable	*F*-test	df	*p*-value
(A) Ψ_{md}			
Ψ_{pd}	5.12	(1, 74)	.03*
Treatment	0.99	(3, 74)	.40
(B) $\Delta\Psi$			
Treatment	0.81	(3, 75)	.49
(C) Ψ_{md}			
Ψ_{hf}	40.5	(1, 73)	<.00001***
Treatment	7.5	(3, 5.4)	.02*
(D) S^{ws}			
Treatment	7.5	(3, 5.4)	<.00001***

4.2 | Sensitivity of the proposed metric and comparison against existing metrics

We also asked whether S^{ws} is sensitive to water status regulation in response to experimental VPD manipulations (question 2). We found that *J. monosperma* regulated water status loosely at both daily and seasonal time scales in the SUMO experiment. Stringency against VPD was also weaker in *J. monosperma* (Figure 4), reflecting the strong seasonal decline in Ψ_{md} with Ψ_{hf} or Ψ_{pd} in this species. Conversely, the regulation against VPD was stricter in *P. edulis*, as evidenced by the fact that Ψ_{md} showed a much more constrained response with Ψ_{hf} despite substantial increases in VPD at low Ψ_{hf}. This difference between the two species contrasts both with the deeper rooting of juniper (Plaut et al., 2012) and with regulation against damage thresholds such as xylem P50 or percentage losses in conductivity, which instead showed no differences across species in response to heating (McDowell et al., 2019). It is however consistent with the generally lower safety margins from critically low transpiration in pine relative to juniper (Plaut et al., 2012). Similar conclusions can be drawn from the experiment with *E. tereticornis*. In this case, the control against VPD effects was entirely dominant, which is hardly surprising, given the deep rooting patterns of this species and the consequent limited impacts of the applied drought treatment (Aspinwall et al., 2016; Drake et al., 2016). Overall, these dynamics may partly reflect traditional effects linked to exposure to embolism linked to soil drought, but they may also reflect some of the additional mechanisms and processes mentioned above acting at daily time scale.

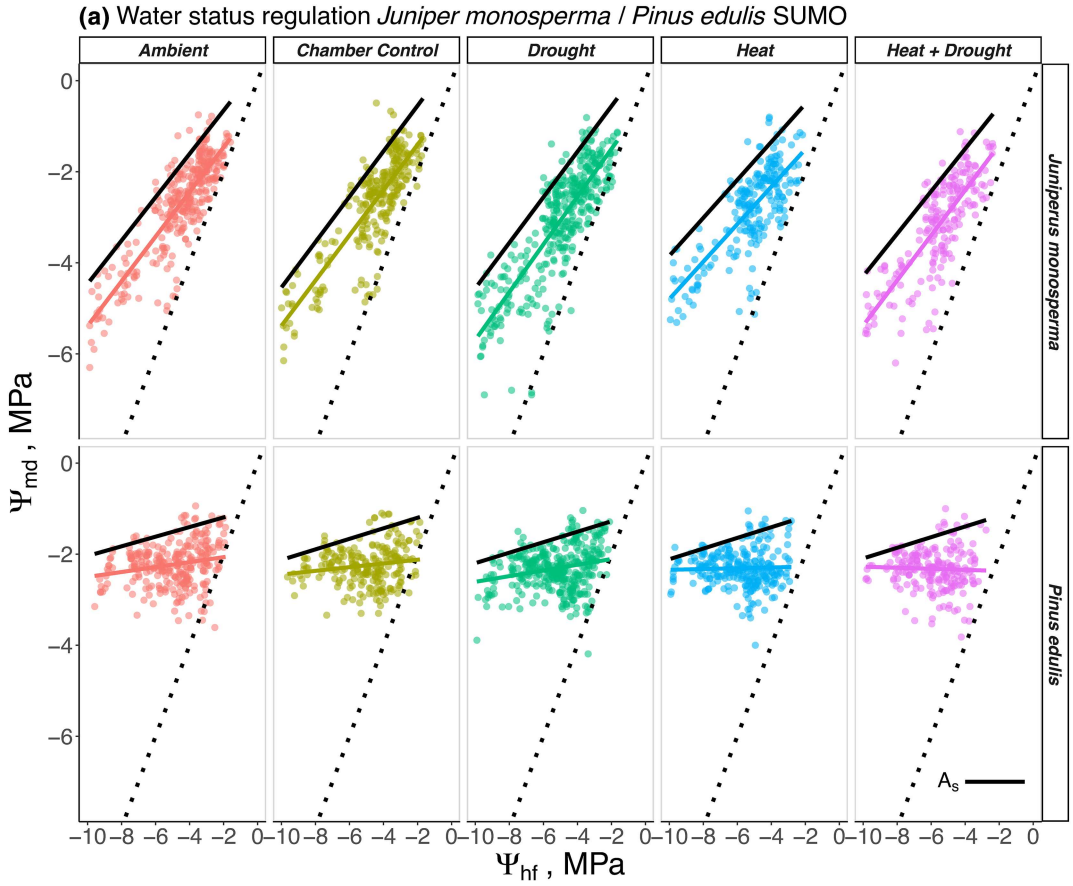

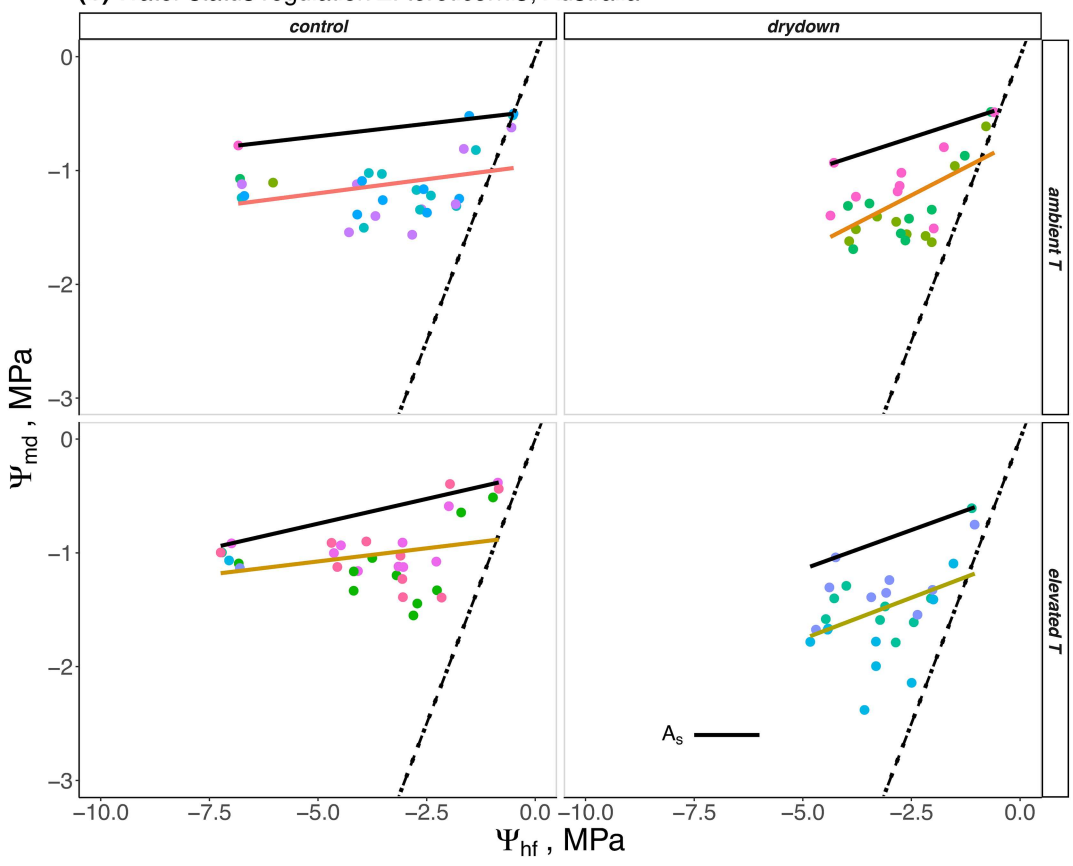

FIGURE 3 Plots of midday leaf water potential Ψ_{md} against the hydraulic effect Ψ_{hf} (i.e., the combined hydraulic 'forcing' by Ψ_{soil} plus VPD), for (a) the SUMO (top) and (b) the Australian WTC experiment (bottom). Plots are given separately by species and treatment (top) and treatment combinations (bottom). On both panels, black lines (marked A_s) give the upper 95% quantiles delimiting the regulation stringency area (contained between the 1:1 and the A_s line); the linear regression lines for each treatment combination are given instead by coloured lines. The dotted line is the 1:1 line.

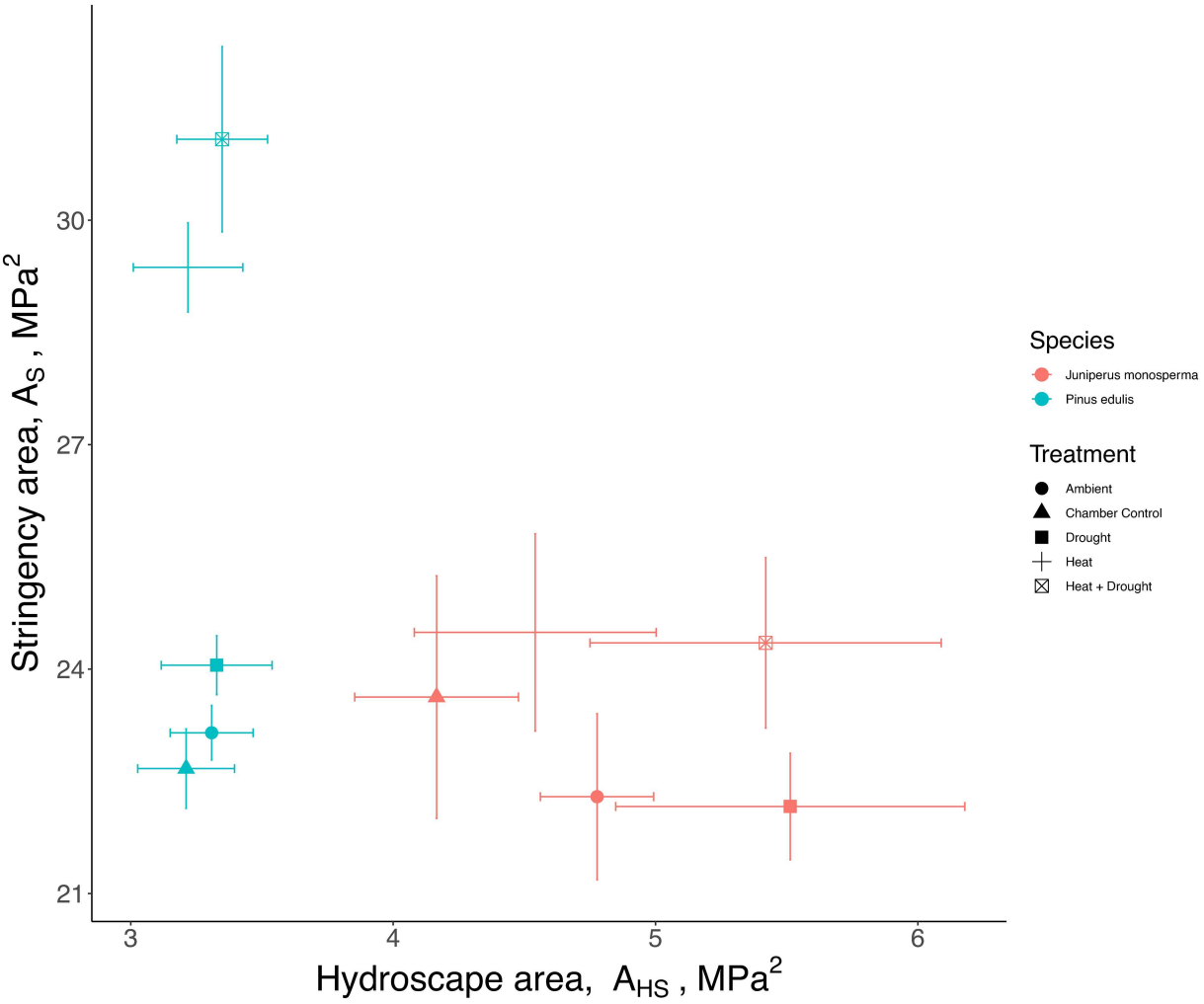

FIGURE 4 Plots of regulation stringency (A_S) against hydroscape area (A_{HS}) for the different species and treatment combinations at the SUMO experiment. Symbols and bars refer to point estimates of the mean and standard errors across individuals for each species/treatment combination.

Compared to traditional isohydry metrics (σ, ΔΨ and the hydroscape area), the stringency metric S^{ws} detected responses to experimental manipulations of water availability and water demand in a much more sensitive manner (Tables 1 and 2; Figure 4; Figure S1). Existing indices that fail to isolate VPD effects likely over-emphasise responses of Ψ_{leaf} to soil drought, consistent with the classic iso/anisohydric interpretation. However, an examination of regulation stringency, that is, S^{ws} and S_{VPD}, shows that VPD responses are strongly involved. This is apparent from the differences in the proportion of Ψ_{hf} caused by VPD at negative Ψ_{hf} across the two species at SUMO (Figure 5), the differences in Ψ_{hf} and regulation stringency for Heat and Heat+Drought relative to Control (Figure 6) and the generally high Ψ_{hf} caused by VPD across all treatments.

4.3 | Understanding and quantifying the effect of VPD on Ψ_{md}

The magnitude of the potential effects of VPD depends on $\widehat{\frac{g_{tot}}{k_L}}$ and therefore varies depending on vegetation characteristics. Provided time series of plant water status and VPD are available, this composite trait is retrieved from the data and effectively calibrates the S^{ws} metric. Its variability over space and time provides meaningful information. High values of $\widehat{\frac{g_{tot}}{k_L}}$ will always amplify the effects of VPD on Ψ_{hf} and therefore using the 95th percentile will always be more conservative than using the 99th percentile of the distribution of Ψ_{hf}. The 99% quantiles of $\widehat{\frac{g_{tot}}{k_L}}$ varied from 1.15 in *J. monosperma*, 1.50

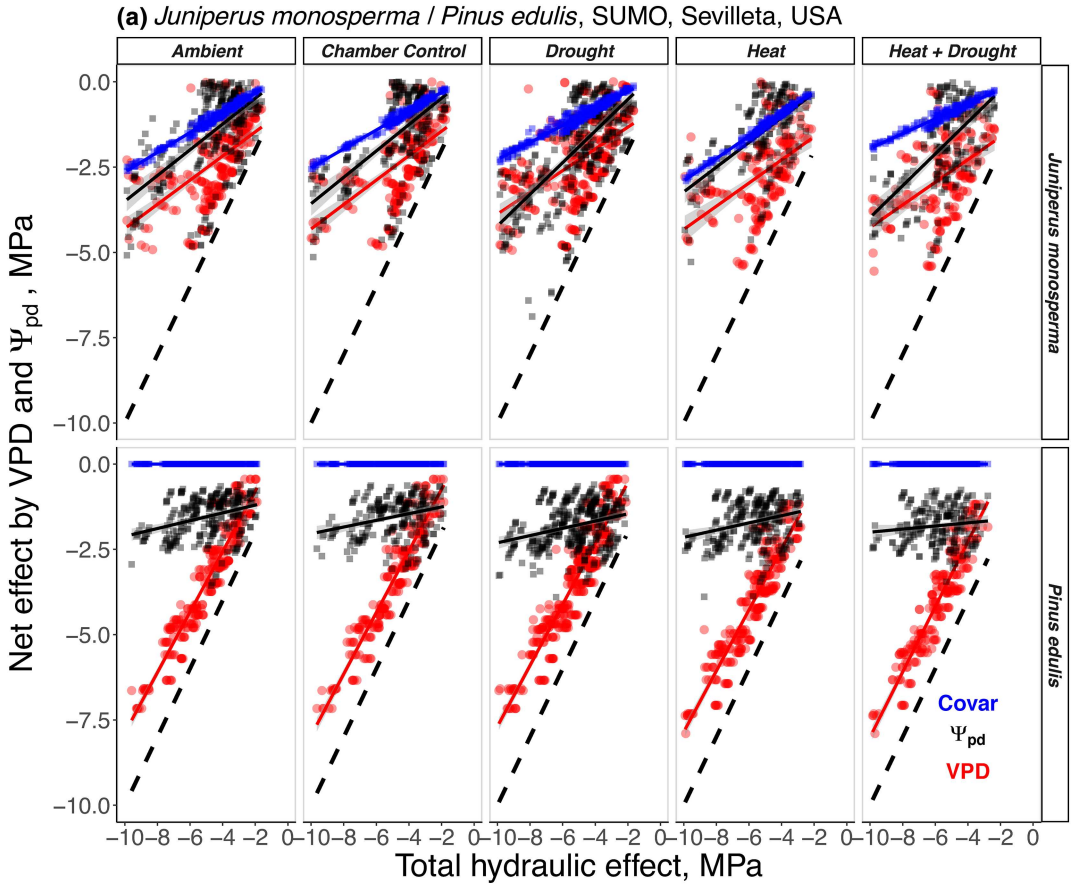

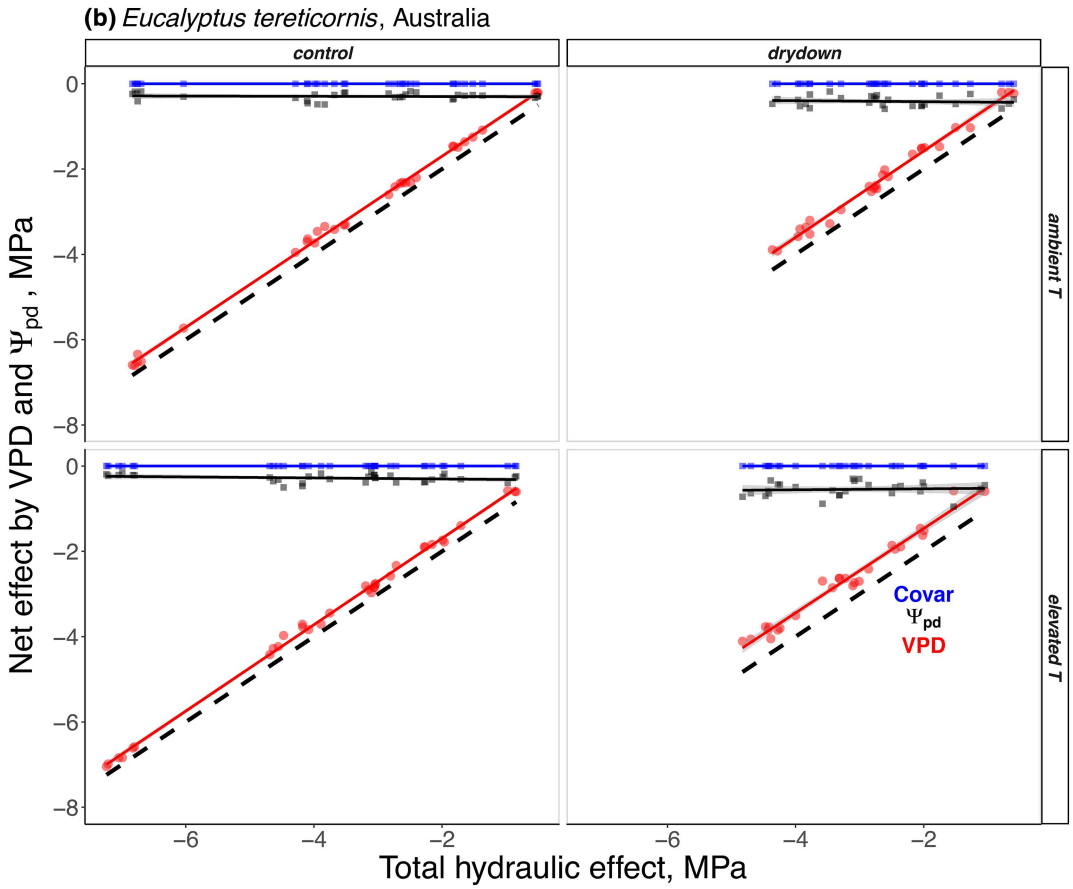

FIGURE 5 Partitioning of hydraulic effect caused by VPD (red) and Ψ_{pd} (black) and covariation between the two (blue symbols) against the total hydraulic effect, for (a) the SUMO (top) and (b) the Australian WTC experiment (bottom). Plots are given separately by species and treatment (top) and treatment combination (bottom). Continuous regression lines give the best fit lines. The black dashed line is the 1:1 line (i.e., the sum of the three components of the total hydraulic effect). The more negative values in some of the sampling dates for the control relative to drydown treatments in the *Eucalyptus tereticornis* experiment are caused by differences in the sampling dates between treatments through the course of the study.

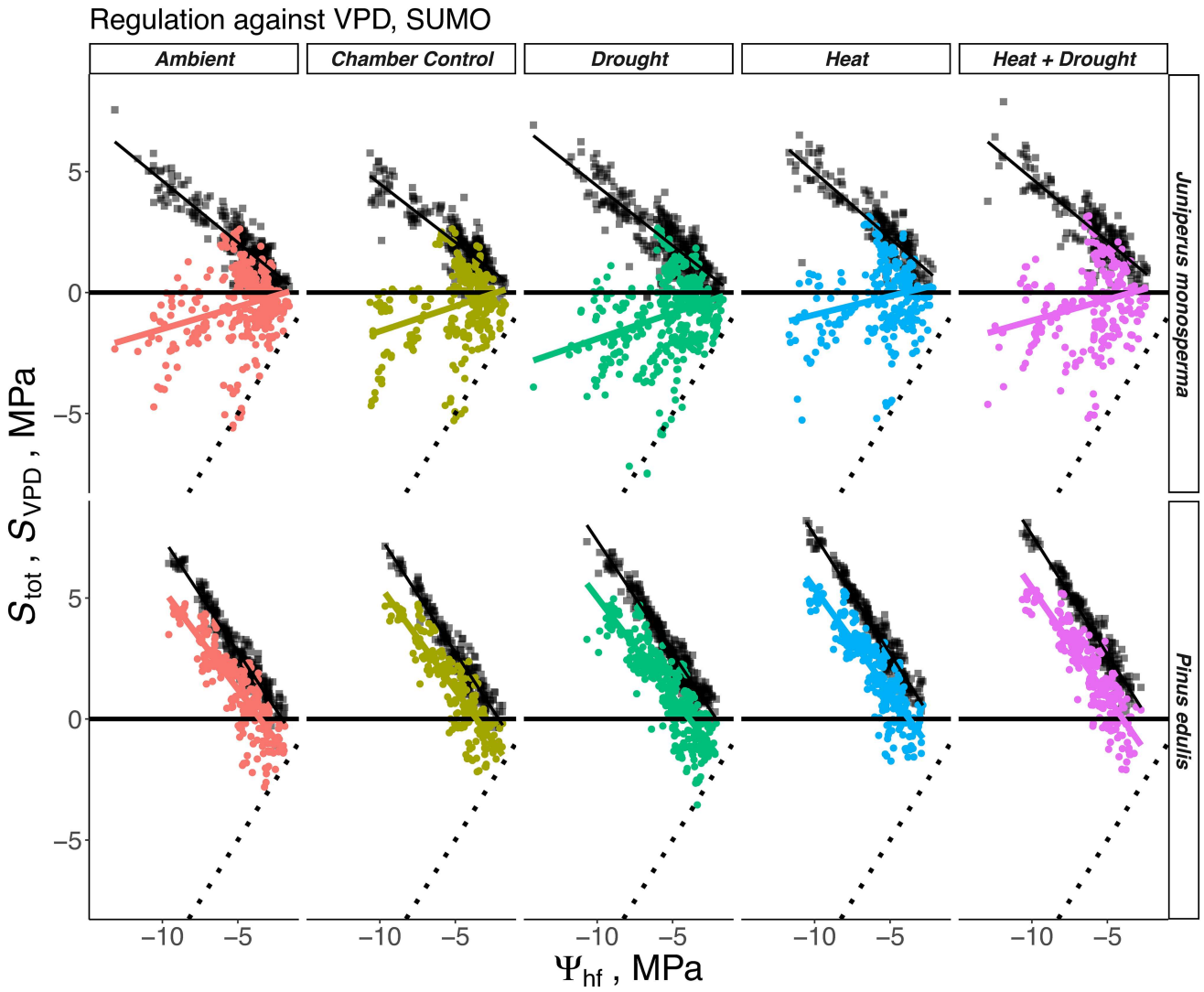

FIGURE 6 Plots of total regulation stringency (black points and regression line) and regulation stringency against VPD only (coloured points and regression lines) plotted against the total hydraulic effect Ψ_{hf} for the different treatment combinations in *Juniperus monosperma* and *Pinus edulis* at the SUMO experiment. Note that while total regulation is very seldom negative, net regulation against VPD can be negative (often, under conditions of high soil water availability and low VPD).

in *P. edulis* to 1.28 in *E. tereticornis*. For the SUMO test case, using values of $\widehat{\frac{g_{tot}}{k_L}}$ for each tree extrapolated to reference VPD and Ψ_{pd}, we explored whether $\widehat{\frac{g_{tot}}{k_L}}$ varied by treatment. The significant reductions found for this ratio in *P. edulis* in the drought and heating treatments may reflect adjustments to maintain Ψ_{hf} within a constrained range despite chamber heating. Previous work at the site suggested adjustments to heating occurred in foliar phenology and morphology (Grossiord, Sevanto, Adams, et al., 2017), stomatal sensitivity to VPD in both species and reference stomatal conductance and saturated leaf-specific conductivity in juniper (Grossiord, Sevanto, Borrego, et al., 2017; McDowell et al., 2019) and water uptake depth in juniper (Grossiord, Sevanto, Dawson, et al., 2017). Adjustments were not found in leaf-sapwood ratios (McBranch et al., 2019), or saturated leaf-specific conductivity in pine (Grossiord, Sevanto, Borrego, et al., 2017) or the s slope (McDowell et al., 2019), as also reported here. The reported reduction in stomatal sensitivity to VPD under heating allowed *P. edulis* to maintain stomatal conductance and sap flux density similar to control (Garcia-Forner et al., 2016; Grossiord,

Sevanto, Borrego, et al., 2017). Interestingly, higher values of water status regulation stringency were apparent in the treatments that generated high VPD in both species, despite the diversity of potential mechanisms mentioned above.

A minimum sample size is required to obtain unbiased estimates of $\widehat{\frac{g_{tot}}{k_L}}$. Estimating a reference from the data using quantiles is simpler and more robust than estimating the extremes of a distribution, because quantiles are not dependent on sampling intensity in the same way as the extremes of a distribution (e.g., (Martínez-Vilalta et al., 2021) for minimum Ψ_{md}). Assuming the SUMO experiment to be representative, a reasonable accuracy and precision in the estimates of Ψ_{hf} and proportion of the total effect by VPD can be obtained with a minimum of 50 values (across replicated trees and dates within each treatment combination). This equates to a monthly sampling schedule for a year across 4–5 individuals. This is not always achieved in physiological studies. For example, in a recently published database of Ψ_{min} (Martínez-Vilalta et al., 2021), only 43 studies have at least 25 sampling dates, and 33 studies at least 50 sampling dates out of 115 time series (although having individual-level data alleviates the problem). The Australian WTC on Eucalyptus did not achieve this minimum required sample size when broken down by treatments (cf., Figure 2). We were consequently unable to calculate a number of metrics for this case study (stringency and hydroscape area) and highlighted the problems existing in some of the other metrics (e.g., sigma). The sample size requirement of $n \geq 50$ is easily obtained in physiological studies based on psychrometry and in remote sensing studies of canopy water content, assuming a sufficiently long experiment to cover a range of conditions. Note, however that applying this method also requires co-occurring VPD time series.

Changes in how $\widehat{\frac{g_{tot}}{k_L}}$ is defined (multiple regression to estimate the ratio at reference values of VPD and Ψ_{pd} versus empirical distribution quantiles) had relatively minor effects on subsequent estimations of Ψ_{hf} and stringency. The first (multiple regression) method obtains estimates under identical conditions across treatments but possibly obtained by extrapolation. It additionally relies on the goodness-of-fit of the regression. In our case, multiple regressions were significant for most combinations, but predictions suffered from significant noise and bias in some cases. The second method produces estimates that are inherently more stable given sufficient sample sizes but obtained under different VPD and Ψ_{soil} conditions for each treatment. Here, $\widehat{\frac{g_{tot}}{k_L}}$ values obtained for each treatment separately without adjusting for different environmental conditions primarily reflected the environmental conditions under which they were obtained (i.e., lower conductances under drought and heating). Consequently, approximation of the maximum $\widehat{\frac{g_{tot}}{k_L}}$ was obtained only by either pooling across treatments or by using Control values. When long-term adjustments of the vegetation to experimental manipulations are suspected, the multiple regression approach allows to obtain estimates of the maxima separately by treatment, avoiding confounding effects of different local environments.

Because of land-atmosphere feedbacks, reduced soil water availability during droughts is often coupled with higher values of atmospheric VPD. This coupling is implicitly considered in the definition of Ψ_{hf} in Equation (4). At SUMO (Figure 5), the two components of Ψ_{hf} co-varied over time in *J. monosperma*, but not in *P. edulis*, because of the much more constrained range of variability in Ψ_{pd} compared to juniper (not shown). Hence, the importance of the seasonal covariation between VPD and Ψ_{soil}, when seen through the lens of the perceived level of soil water stress by the plant (i.e., Ψ_{pd}), varies as a function of plant rooting strategies. Although this conclusion was confirmed in the Australian experiment, it is likely that the underlying mechanisms vary. In the case of *P. edulis*, like in other pine species, hydraulic disconnection between plant roots and soil is a major component of the maintenance of a seasonal minimum Ψ_{md}, while the relevance of this mechanism at the daily time scale is not well studied. In the case of the Australian experiment, lack of seasonal covariation between VPD and Ψ_{soil} was largely the result of the deep-rooting habit of *E. tereticornis*.

Although Ψ_{pd} was considered here identical to Ψ_{soil}, the relationship between the two variables is complex. Firstly, nighttime transpiration can reduce Ψ_{pd} below Ψ_{soil} (Donovan et al., 1999; Kangur et al., 2017). Secondly, Equation (1) implicitly assumes that Ψ_{soil} at midday is identical to Ψ_{soil} at predawn (Binks et al., 2022). This may not be justified in cases of large transpiration-induced disequilibria in soil water potentials around plant roots, a situation observed in crop plants and on sandier substrates (Cai et al., 2022). More importantly, employing Ψ_{pd} as opposed to Ψ_{soil} is justified when availability of soil water potential data is limited, as was the case here for physiological experiments manipulating VPD levels (Novick et al., 2022). A complete partitioning of soil versus atmospheric hydraulic effects should consider the possibility that plant roots disconnect from and re-connect to the soil also at daily time scale. Under such circumstances, regulation against soil drought will be amplified if Ψ_{soil} is considered. An expression containing Ψ_{soil} instead of Ψ_{pd} in Equation (1) would then depend on a variable like $\widehat{\frac{g_{tot}}{k_L}}$, but incorporating the contribution of rhizosphere resistances. Such a variable would include plant traits but also properties such as soil texture and structure, giving an equivalent site-dependent reference state.

4.4 | Water potential regulation under different conceptual frameworks

We asked how the regulation of water status against high VPD compares with the regulation against negative Ψ_{pd} (question 3). We showed that plant control against the hydraulic effects of VPD was at least as important as the control against Ψ_{pd}. Remarkably at SUMO, both Ψ_{hf} and regulation in the Heat treatments ranked higher than the equivalent properties under Drought, reinforcing the thermodynamic significance of VPD against soil drought for both species at SUMO.

The curvilinear relationships of Ψ_{md} with Ψ_{hf} suggest a progressive decline towards a seasonal minimum Ψ_{md} that reflects the sum of soil and atmospheric hydraulic effects. Employing this relationship to estimate the absolute seasonal Ψ_{min} is tempting. However, it is likely that the relationship changes shape beyond turgor loss

point TLP. This is understandable on the grounds that the distribution of $\frac{g_{tot}}{k_L}$ may change once leaf conductance is entirely limited by leaf minimum conductance. Turgor loss can also affect Ψ_{leaf} directly, although these species have been shown to undergo substantial seasonal adjustments in TLP effectively preventing turgor loss (Meinzer et al., 2014). It is also possible that changes in the distribution of $\frac{g_{tot}}{k_L}$ may partly be controlled by hydraulic conductance or belowground traits, such as root-soil contact. Further work is required to explore these ideas and test whether changes in the distribution of $\frac{g_{tot}}{k_L}$ relate to thresholds beyond which physiological damage occurs.

Shifting the analysis from the Ψ_{pd}–Ψ_{md} to the Ψ_{hf}–Ψ_{md} space, eliminated regression and boundary lines with extreme values, for example, slopes >1 (Figure 2, bottom panel for the Drydown Elevated treatment). These lines are sometimes characterized as indicating extreme anisohydric behaviour. It is obvious from our analysis that the reason for this apparent behavior is because the hydraulic effects of VPD had not been accounted for (cf., Figures 2 and 3). In addition, for both case studies, values of the Ψ_{hf}–Ψ_{md} regression slopes were always lower than Ψ_{pd}–Ψ_{md} slopes (cf., Figure S1). This can be understood from the definition of regression slope as $b = \frac{Cov(x,y)}{Var(x)}$ and that $Var(\Psi_{pd}) + Var\left(\widehat{\frac{g_{tot}}{K_L}}\,VPD\right) > Var(\Psi_{pd})$ always. The fact that regression slopes in Ψ_{hf}–Ψ_{md} space are likely to always be smaller than σ in turn implies that plants are generally more isohydric than when assessed without considering VPD.

When the hydroscape area A_{HS} (Meinzer et al., 2016) was compared against the area of regulation stringency A_S, a broad negative relationship was obtained (Figure 4). A_{HS} can be written as $A_{HS} \approx \int (\Psi_{pd} - \Psi_{md}) d\Psi_{pd}$. Using Equation (1), assuming that VPD is constant, this can be expressed as $A_{HS} \approx VPD \int \frac{g_{tot}}{k_L} d\Psi_{pd}$. Conversely, $A_S \approx \int (\Psi_{md} - \Psi_{hf}) d\Psi_{hf} = VPD \int \left(\widehat{\frac{g_{tot}}{k_L}} - \frac{g_{tot}}{k_L}\right) d\Psi_{pd}$, suggesting that A_{HS} and A_S should be negatively related, as found. However, VPD is never constant. If VPD varies over time, the relationship between the two areas will change, because $VPD\widehat{\frac{g_{tot}}{k_L}}$ will vary over time. It is therefore likely that this relationship breaks down across a wider range of species and VPD conditions and the inverse relationship reported in Figure 4 should therefore be taken with caution. Like the case for the hydroscape area, under the assumption of constant VPD, the slope of the regression between Ψ_{hf} against Ψ_{md} retrieves σ (not shown). Under the same assumption, $S_{\Psi_{pd}}$ retrieves (with the reversed sign) the usual daily water potential difference ΔΨ (Klein, 2014; Martínez-Vilalta & Garcia-Forner, 2017). Hence, the regulation stringency metrics presented here generalize existing metrics. Conversely, determining the effects of the seasonal variability in VPD is important, because existing isohydry metrics implicitly assume VPD to be constant.

4.5 | Time-varying regulation metrics versus species-level properties

One of the three metrics presented here, namely, stringency S^{WS}, can vary at short time scales and therefore be affected by instantaneous abiotic and biotic conditions. Conversely, the other two metrics (A_S and the slope of Ψ_{hf}–Ψ_{md} relationship) are time-averaged and integrate across the spectrum of variability of the drivers. Because of their sensitivity to local conditions, it is likely that instantaneous metrics can provide novel insights compared to time-averaged metrics. Beyond these three metrics, the maximum value of the distributions of S^{WS} may also be significant since maximum stringency is likely constrained. When Ψ_{hf} becomes very negative, unregulated surface water losses will force Ψ_{md} to decline and therefore will lead to an upper limit in stringency. In the SUMO case study, the 95% quantiles of regulation were higher in Heat and Heat+Drought, suggesting that this maximum had not been reached, at least not in Ambient and Drought. Identification of these critical thresholds using the metrics proposed here should be easier than for thresholds calculated without using a reference null model.

5 | CONCLUSIONS

We presented a novel metric for the quantification of water status regulation stringency. We showed that this metric is more sensitive to manipulations of VPD compared to existing metrics. We also showed that regulation against high VPD is a very large component of regulation of plant water status, in two out of three cases the dominant one. Metrics for the quantification of water status regulation in vivo are complementary to metrics of water use regulation and to mechanistic hydraulic traits, since ultimately the behaviour of field metrics needs to be interpreted in the context of regulation relative to hydraulic damage traits. Increasingly, ecosystem-level models are becoming hydraulically enabled to predict plant water status as well as plant to ecosystem-scale water fluxes (Eller et al., 2020; Kennedy et al., 2019; Li et al., 2021; Sabot et al., 2020). These hydraulically enabled models can be less skilful in predicting plant water status than water use (De Cáceres et al., 2021; Eller et al., 2020; Kennedy et al., 2019; Sabot et al., 2022; Venturas et al., 2018). The metrics developed here can be useful in teasing apart the reasons of this variable performance and in aiding interpretation of remote sensing time series and physiological field monitoring.

AUTHOR CONTRIBUTIONS

Maurizio Mencuccini: Conceptualization; formal analysis; methodology; visualization; writing – original draft. **William R. L. Anderegg:** Conceptualization; writing – review and editing. **Oliver Binks:** Conceptualization; writing – review and editing. **Thorsten Knipfer:** Conceptualization; writing – review and editing. **Alexandra G. Konings:** Conceptualization; writing – review and editing. **Kim Novick:** Conceptualization; investigation; resources; writing – review and editing. **Rafael Poyatos:** Conceptualization; resources; writing – review and editing. **Jordi Martínez-Vilalta:** Conceptualization; methodology; resources; writing – review and editing.

ACKNOWLEDGEMENTS

MM acknowledges support by the Spanish Ministry of Economy and Competitiveness (MINECO) via grant PRE2018-086096 (DRESS) and

EU-2020 programme via grant 862221 (FORGENIUS). TK acknowledges funding from Natural Sciences and Engineering Research Council of Canada (NSERC). AGK was funded by the Alfred P. Sloan foundation.

CONFLICT OF INTEREST STATEMENT

None declared.

DATA AVAILABILITY STATEMENT

The data that support the findings of this study are openly available in [SUMO Leaf Water Potential. Vegetation Survival-Mortality (SUMO), ESS-DIVE repository. Dataset] at [https://www.osti.gov/dataexplorer/biblio/dataset/1439886], reference number [DOI: https://doi.org/10.15485/1439886]. SUMO Micrometeorology. Vegetation Survival-Mortality (SUMO), ESS-DIVE repository. Dataset. accessed via https://data.ess-dive.lbl.gov/datasets. reference number [https://doi.org/10.15485/1454272] and at Figshare at [https://figshare.com/articles/dataset/Drake_NewPhyt_2016_WTC3_RtoGPP_forfigshare_zip/3122104/1].

ORCID

William R. L. Anderegg https://orcid.org/0000-0001-6551-3331
Alexandra G. Konings https://orcid.org/0000-0002-2810-1722
Kim Novick https://orcid.org/0000-0002-8431-0879

REFERENCES

Anderegg, W. R. L., Wolf, A., Arango-Velez, A., Choat, B., Chmura, D. J., Jansen, S., Kolb, T., Li, S., Meinzer, F., Pita, P., de Dios, V. R., Sperry, J. S., Wolfe, B. T., & Pacala, S. (2017). Plant water potential improves prediction of empirical stomatal models. *PLoS One*, *12*, 1–17.

Aspinwall, M. J., Drake, J. E., Campany, C., Vårhammar, A., Ghannoum, O., Tissue, D. T., Reich, P. B., & Tjoelker, M. G. (2016). Convergent acclimation of leaf photosynthesis and respiration to prevailing ambient temperatures under current and warmer climates in *Eucalyptus tereticornis*. *New Phytologist*, *212*, 354–367.

Bakken, G. S., Santee, W. R., & Erskine, D. J. (1985). Operative and standard operative temperature: Tools for thermal energetics studies. *American Zoologist*, *25*, 933–943.

Binks, O., Cernusak, L. A., Liddell, M., Bradford, M., Coughlin, I., Carle, H., Bryant, C., Dunn, E., Oliveira, R., Mencuccini, M., & Meir, P. (2022). Forest system hydraulic conductance: Partitioning tree and soil components. *New Phytologist*, *233*, 1667–1681.

Cai, G., Ahmed, M. A., Abdalla, M., & Carminati, A. (2022). Root hydraulic phenotypes impacting water uptake in drying soils. *Plant, Cell & Environment*, *45*, 650–663.

Caldeira, C. F., Jeanguenin, L., Chaumont, F., & Tardieu, F. (2014). Circadian rhythms of hydraulic conductance and growth are enhanced by drought and improve plant performance. *Nature Communications*, *5*, 5365.

De Cáceres, M., Mencuccini, M., Martin-StPaul, N., Limousin, J.-M., Coll, L., Poyatos, R., Cabon, A., Granda, V., Forner, A., Valladares, F., & Martínez-Vilalta, J. (2021). Unravelling the effect of species mixing on water use and drought stress in Mediterranean forests: A modelling approach. *Agricultural and Forest Meteorology*, *296*, 108233.

Donovan, L. A., Grisé, D. J., West, J. B., Pappert, R. A., Alder, N. N., & Richards, J. H. (1999). Predawn disequilibrium between plant and soil water potentials in two cold-desert shrubs. *Oecologia*, *120*, 209–217.

Drake, J. E., Tjoelker, M. G., Aspinwall, M. J., Reich, P. B., Barton, C. V. M., Medlyn, B. E., & Duursma, R. A. (2016). Does physiological acclimation to climate warming stabilize the ratio of canopy respiration to photosynthesis? *New Phytologist*, *211*, 850–863.

Ehlert, C., Maurel, C., Tardieu, F., & Simonneau, T. (2009). Aquaporin-mediated reduction in maize root hydraulic conductivity impacts cell turgor and leaf elongation even without changing transpiration. *Plant Physiology*, *150*, 1093–1104.

Eller, C. B., Rowland, L., Mencuccini, M., Rosas, T., Williams, K., Harper, A., Medlyn, B. E., Wagner, Y., Klein, T., Teodoro, G. S., Oliveira, R. S., Matos, I. S., Rosado, B. H. P., Fuchs, K., Wohlfahrt, G., Montagnani, L., Meir, P., Sitch, S., & Cox, P. M. (2020). Stomatal optimization based on xylem hydraulics (SOX) improves land surface model simulation of vegetation responses to climate. *New Phytologist*, *226*, 1622–1637.

Feng, X., Ackerly, D. D., Dawson, T. E., Manzoni, S., McLaughlin, B., Skelton, R. P., Vico, G., Weitz, A. P., & Thompson, S. E. (2019). Beyond isohydricity: The role of environmental variability in determining plant drought responses. *Plant, Cell & Environment*, *42*, 1104–1111.

Flo, V., Martínez-Vilalta, J., Mencuccini, M., Granda, V., Anderegg, W. R. L., & Poyatos, R. (2021). Climate and functional traits jointly mediate tree water-use strategies. *New Phytologist*, *231*, 617–630.

Fu, X., & Meinzer, F. C. (2019). Metrics and proxies for stringency of regulation of plant water status (iso/anisohydry): A global data set reveals coordination and trade-offs among water transport traits. *Tree Physiology*, *39*, 122–134.

Garcia-Forner, N., Adams, H. D., Sevanto, S., Collins, A. D., Dickman, L. T., Hudson, P. J., Zeppel, M. J. B., Jenkins, M. W., Powers, H., Martínez-Vilalta, J., & Mcdowell, N. G. (2016). Responses of two semiarid conifer tree species to reduced precipitation and warming reveal new perspectives for stomatal regulation. *Plant, Cell & Environment*, *39*, 38–49.

Grossiord, C., Buckley, T. N., Cernusak, L. A., Novick, K. A., Poulter, B., Siegwolf, R. T. W., Sperry, J. S., & McDowell, N. G. (2020). Plant responses to rising vapor pressure deficit. *New Phytologist*, *226*, 1550–1566.

Grossiord, C., Sevanto, S., Adams, H. D., Collins, A. D., Dickman, L. T., McBranch, N., Michaletz, S. T., Stockton, E. A., Vigil, M., & McDowell, N. G. (2017). Precipitation, not air temperature, drives functional responses of trees in semi-arid ecosystems. *Journal of Ecology*, *105*, 163–175.

Grossiord, C., Sevanto, S., Borrego, I., Chan, A. M., Collins, A. D., Dickman, L. T., Hudson, P. J., Mcbranch, N., Michaletz, S. T., Pockman, W. T., Ryan, M., Vilagrosa, A., & McDowell, N. G. (2017). Tree water dynamics in a drying and warming world. *Plant, Cell & Environment*, *40*, 1861–1873.

Grossiord, C., Sevanto, S., Dawson, T. E., Adams, H. D., Collins, A. D., Dickman, L. T., Newman, B. D., Stockton, E. A., & McDowell, N. G. (2017). Warming combined with more extreme precipitation regimes modifies the water sources used by trees. *New Phytologist*, *213*, 584–596.

Guo, J. S., Hultine, K. R., Koch, G. W., Kropp, H., & Ogle, K. (2019). Temporal shifts in iso/anisohydry revealed from daily observations of plant water potential in a dominant desert shrub. *New Phytologist*, *225*, 713–726.

Guo, J. S., & Ogle, K. (2019). Antecedent soil water content and vapor pressure deficit interactively control water potential in Larrea tridentata. *New Phytologist*, *221*, 218–232.

Hochberg, U., Rockwell, F. E., Holbrook, N. M., & Cochard, H. (2018). Iso/anisohydry: A plant–environment interaction rather than a simple hydraulic trait. *Trends in Plant Science*, *23*, 112–120.

Holtzman, N. M., Anderegg, L. D. L., Kraatz, S., Mavrovic, A., Sonnentag, O., Pappas, C., Cosh, M. H., Langlois, A., Lakhankar, T., Tesser, D., Steiner, N., Colliander, A., Roy, A., & Konings, A. G. (2021). L-band

vegetation optical depth as an indicator of plant water potential in a temperate deciduous forest stand. *Biogeosciences*, *18*, 739–753.

Kangur, O., Kupper, P., & Sellin, A. (2017). Predawn disequilibrium between soil and plant water potentials in light of climate trends predicted for northern Europe. *Regional Environmental Change*, *17*, 2159–2168.

Kannenberg, S. A., Guo, J. S., Novick, K. A., Anderegg, W. R. L., Feng, X., Kennedy, D., Konings, A. G., Martínez-Vilalta, J., & Matheny, A. M. (2022). Opportunities, challenges and pitfalls in characterizing plant water-use strategies. *Functional Ecology*, *36*, 24–37.

Kennedy, D., Swenson, S., Oleson, K. W., Lawrence, D. M., Fisher, R., Lola da Costa, A. C., & Gentine, P. (2019). Implementing plant hydraulics in the community land model, version 5. *Journal of Advances in Modeling Earth Systems*, *11*, 485–513.

Klein, T. (2014). The variability of stomatal sensitivity to leaf water potential across tree species indicates a continuum between isohydric and anisohydric behaviours (S Niu, Ed.). *Functional Ecology*, *28*, 1313–1320.

Knipfer, T., Bambach, N., Hernandez, M. I., Bartlett, M. K., Sinclair, G., Duong, F., Kluepfel, D. A., & McElrone, A. J. (2020). Predicting stomatal closure and turgor loss in Woody plants using predawn and midday water potential. *Plant Physiology*, *184*, 881–894.

Koenker, R. (2005). *Quantile regression*. Cambridge University Press.

Konings, A. G., Rao, K., & Steele-Dunne, S. C. (2019). Macro to micro: Microwave remote sensing of plant water content for physiology and ecology. *New Phytologist*, *223*, 1166–1172.

Konings, A. G., Saatchi, S. S., Frankenberg, C., Keller, M., Leshyk, V., Anderegg, W. R. L., Humphrey, V., Matheny, A. M., Trugman, A., Sack, L., Agee, E., Barnes, M. L., Binks, O., Cawse-Nicholson, K., Christoffersen, B. O., Entekhabi, D., Gentine, P., Holtzman, N. M., Katul, G. G., … Zuidema, P. A. (2021). Detecting forest response to droughts with global observations of vegetation water content. *Global Change Biology*, *27*, 6005–6024.

Li, L., Yang, Z., Matheny, A. M., Zheng, H., Swenson, S. C., Lawrence, D. M., Barlage, M., Yan, B., McDowell, N. G., & Leung, L. R. (2021). Representation of plant hydraulics in the Noah-MP land surface model: Model development and multiscale evaluation. *Journal of Advances in Modeling Earth Systems*, *13*, e2020MS002214.

Lin, Y. S., Medlyn, B. E., Duursma, R. A., Prentice, I. C., Wang, H., Baig, S., Eamus, D., De Dios, V. R., Mitchell, P., Ellsworth, D. S., Op de Beeck, M., Wallin, G., Uddling, J., Tarvainen, L., Linderson, M.-L., Cernusak, L. A., Nippert, J. B., Ocheltree, T. W., Tissue, D. T., … Wingate, L. (2015). Optimal stomatal behaviour around the world. *Nature Climate Change*, *5*, 459–464.

Martínez-Vilalta, J., & Garcia-Forner, N. (2017). Water potential regulation, stomatal behaviour and hydraulic transport under drought: Deconstructing the iso/anisohydric concept. *Plant, Cell & Environment*, *40*, 962–976.

Martínez-Vilalta, J., Poyatos, R., Aguade, D., Retana, J., & Mencuccini, M. (2014). A new look at water transport regulation in plants. *New Phytologist*, *204*, 105–115.

Martínez-Vilalta, J., Santiago, L. S., Poyatos, R., Badiella, L., Cáceres, M., Aranda, I., Delzon, S., Vilagrosa, A., & Mencuccini, M. (2021). Towards a statistically robust determination of minimum water potential and hydraulic risk in plants. *New Phytologist*, *232*, 404–417.

McBranch, N. A., Grossiord, C., Adams, H., Borrego, I., Collins, A. D., Dickman, T., Ryan, M., Sevanto, S., & McDowell, N. G. (2019). Lack of acclimation of leaf area: Sapwood area ratios in piñon pine and juniper in response to precipitation reduction and warming. *Tree Physiology*, *39*, 135–142.

McDowell, N. G., Grossiord, C., Adams, H. D., Pinzón-Navarro, S., Mackay, D. S., Breshears, D. D., Allen, C. D., Borrego, I., Dickman, L. T., Collins, A., Gaylord, M., McBranch, N., Pockman, W. T., Vilagrosa, A., Aukema, B., Goodsman, D., & Xu, C. (2019). Mechanisms of a coniferous woodland persistence under drought and heat. *Environmental Research Letters*, *14*, 045014.

Meinzer, F. C., Woodruff, D. R., Marias, D. E., Mcculloh, K. A., & Sevanto, S. (2014). Dynamics of leaf water relations components in co-occurring iso- and anisohydric conifer species. *Plant, Cell & Environment*, *37*, 2577–2586.

Meinzer, F. C., Woodruff, D. R., Marias, D. E., Smith, D. D., McCulloh, K. A., Howard, A. R., & Magedman, A. L. (2016). Mapping 'hydroscapes' along the iso- to anisohydric continuum of stomatal regulation of plant water status. *Ecology Letters*, *19*, 1343–1352.

Mencuccini, M., Manzoni, S., & Christoffersen, B. (2019). Modelling water fluxes in plants: From tissues to biosphere. *New Phytologist*, *222*, 1207–1222.

Novick, K. A., Ficklin, D. L., Baldocchi, D., Davis, K. J., Ghezzehei, T. A., Konings, A. G., MacBean, N., Raoult, N., Scott, R. L., Shi, Y., Sulman, B. N., & Wood, J. D. (2022). Confronting the water potential information gap. *Nature Geoscience*, *15*, 158–164.

Novick, K. A., Konings, A. G., & Gentine, P. (2019). Beyond soil water potential: An expanded view on isohydricity including land–atmosphere interactions and phenology. *Plant, Cell & Environment*, *42*, 1802–1815.

Plaut, J. A., Yepez, E. A., Hill, J., Pangle, R., Sperry, J. S., Pockman, W. T., & Mcdowell, N. G. (2012). Hydraulic limits preceding mortality in a piñon-juniper woodland under experimental drought. *Plant, Cell & Environment*, *35*, 1601–1617.

Prentice, I. C., Dong, N., Gleason, S. M., Maire, V., & Wright, I. J. (2014). Balancing the costs of carbon gain and water transport: Testing a new theoretical framework for plant functional ecology. *Ecology Letters*, *17*, 82–91.

R Development Core Team. (2013). *R: A language and environment for statistical computing*. R Foundation for Statistical Computing.

Rogers, A., Medlyn, B. E., & Dukes, J. S. (2014). Improving representation of photosynthesis in earth system models. *New Phytologist*, *204*, 12–14.

Sabot, M. E. B., De Kauwe, M. G., Pitman, A. J., Medlyn, B. E., Ellsworth, D. S., Martin-StPaul, N. K., Wu, J., Choat, B., Limousin, J., Mitchell, P. J., Rogers, A., & Serbin, S. P. (2022). One stomatal model to rule them all? Toward improved representation of carbon and water exchange in global models. *Journal of Advances in Modeling Earth Systems*, *14*, e2021MS002761.

Sabot, M. E. B., De Kauwe, M. G., Pitman, A. J., Medlyn, B. E., Verhoef, A., Ukkola, A. M., & Abramowitz, G. (2020). Plant profit maximization improves predictions of European forest responses to drought. *New Phytologist*, *226*, 1638–1655.

Scoffoni, C., Kunkle, J., Pasquet-Kok, J., Vuong, C., Patel, A. J., Montgomery, R. A., Givnish, T. J., & Sack, L. (2015). Light-induced plasticity in leaf hydraulics, venation, anatomy, and gas exchange in ecologically diverse Hawaiian lobeliads. *New Phytologist*, *207*, 43–58.

Sevanto, S., Dickman, T. L., Collins, A., Grossiord, C., Adams, H., Borrego, I., & McDowell, N. (2018a). *SUMO micrometeorology*. Vegetation Survival-Mortality (SUMO), ESS-DIVE repository. Dataset. Retrieved from https://data.ess-dive.lbl.gov/datasets

Sevanto, S., Dickman, L. T., Collins, A., Grossiord, C., Adams, H., Borrego, I., & McDowell, N. (2018b). *SUMO leaf water potential*. Vegetation Survival-Mortality (SUMO), ESS-DIVE repository. Dataset.

Shackel, K. (2011). A plant-based approach to deficit irrigation in trees and vines. *HortScience*, *46*, 173–177.

Shackel, K., Moriana, A., Marino, G., Corell, M., Pérez-López, D., Martin-Palomo, M. J., Caruso, T., Marra, F. P., Agüero Alcaras, L. M., Milliron, L., Rosecrance, R., Fulton, A., & Searles, P. S. (2021). Establishing a reference baseline for midday stem water potential in olive and its use for plant-based irrigation management. *Frontiers in Plant Science*, *12*, 1–12.

Sperry, J. S., Venturas, M. D., Anderegg, W. R. L. L., Mencuccini, M., Mackay, D. S., Wang, Y., & Love, D. M. (2017). Predicting stomatal responses to the environment from the optimization of photosynthetic gain and hydraulic cost. *Plant, Cell & Environment*, *40*, 816–830.

Tardieu, F., & Simonneau, T. (1998). Variability among species of stomatal control under fluctuating soil water status and evaporative demand: Modelling isohydric and anisohydric behaviours. *Journal of Experimental Botany*, *49*, 419–432.

Tyree, M. T., & Jarvis, P. G. (1982). Water in tissues and cells. In O. L. Lange, P. S. Nobel, C. B. Osmond, & H. Ziegler (Eds.), *Physiological plant ecology II* (pp. 35–77). Springer-Verlag Berlin Heidelberg.

Venturas, M. D., Sperry, J. S., Love, D. M., Frehner, E. H., Allred, M. G., Wang, Y., & Anderegg, W. R. L. (2018). A stomatal control model based on optimization of carbon gain versus hydraulic risk predicts aspen sapling responses to drought. *New Phytologist*, *220*, 836–850.

Venturas, M. D., Todd, H. N., Trugman, A. T., & Anderegg, W. R. L. (2021). Understanding and predicting forest mortality in the western United States using long-term forest inventory data and modeled hydraulic damage. *New Phytologist*, *230*, 1896–1910.

Whitehead, D., & Jarvis, P. G. (1981). Chapter 2—Coniferous forests and plantations. In T. T. Kozlowski (Ed.), *Woody plant communities* (pp. 49–152). Academic Press.

SUPPORTING INFORMATION

Additional supporting information can be found online in the Supporting Information section at the end of this article.

How to cite this article: Mencuccini, M., Anderegg, W. R. L., Binks, O., Knipfer, T., Konings, A. G., Novick, K., Poyatos, R., & Martínez-Vilalta, J. (2024). A new empirical framework to quantify the hydraulic effects of soil and atmospheric drivers on plant water status. *Global Change Biology*, *30*, e17222. https://doi.org/10.1111/gcb.17222